1 Introduction

The swimming of microscopic organisms has been a rich source of research for decades [1,2]. A natural extension of this research is the design of artificial microswimmers, which could be applied to targeted medication delivery or the autonomous pumping of fluid [3,4]. Biological systems have inspired many of the resulting designs, such as swimmers which mimic spermatozoa by waving a filament under the influence of an external magnetic field [5]. The minimum size of the propulsive filaments required to swim in this way is limited by manufacturing constraints, so miniaturizing the concept is difficult.

Another design, the Janus particle, swims without any mechanical parts or body deformation through a process called self-diffusiophoresis. Named for the Roman two-faced god, the Janus swimmer catalytically reacts with the surrounding fluid differently on each of its two sides, asymmetrically emitting solute into the surrounding fluid [6]. This induces an effective slip velocity over the particle's surface, resulting in movement without the need for an outside energy source [7]. The design can be fabricated by coating one or both halves of a sphere with varying catalytic substances, a procedure which, even at small length scales, is within the reach current manufacturing techniques [8].

The potential applications for microswimmers listed above imply their presence in confined environments such as capillaries or channels, but designing robotic swimmers capable of such tasks will require a much better understanding of the effects of confinement on swimmer motion. Janus particles, given their lack of outside actuation and suitability for miniaturization, are an excellent candidate for further development and have been frequently studied in recent years [3, 4, 6, 8–13]. While experiments and simulations demonstrate rich, varied multi-particle dynamics [9], even single particles display complex behavior when swimming near a boundary [4].

This essay will investigate confinement effects on isolated Janus particles by examining analytical treatments of the swimmers near planar walls, specifically the work of Ibrahim and Liverpool [13] and Crowdy [10]. It will be shown that confinement produces two effects on Janus particles which dominate the interaction. A leading-order repulsion from the boundary is caused by the wall's influence on the solute distribution around the particle, while a rotation of the particle away from the wall is induced by hydrodynamic effects. This combination causes an avoidance of confinement, although certain particle configurations may be susceptible to capture along the wall. A detailed outline follows.

In Section 2, the process of self-diffusiophoresis will be explained in detail, and several results which inform the rest of the essay will be derived. Section 3 will reproduce the work of Golestanian, Liverpool and Ajdari [6] and Ibrahim and Liverpool [13] by examining the motion of a three-dimensional Janus particle in unbounded fluid and near a wall. This analysis will yield several conclusions, but will be unable to explain certain behaviors which have recently been observed in numerical simulations [4]. To rectify this, Section 4 will draw on the work of Crowdy [10] to find an exact solution to the problem in two-dimensions, using complex variables and conformal mapping. The process will yield indirect evidence for the numerical observations. In Section 5, I will use conformal mapping to non-rigorously extend Crowdy's solution to more general environments. Finally, Section 6 will discuss several conclusions and opportunities for future research.

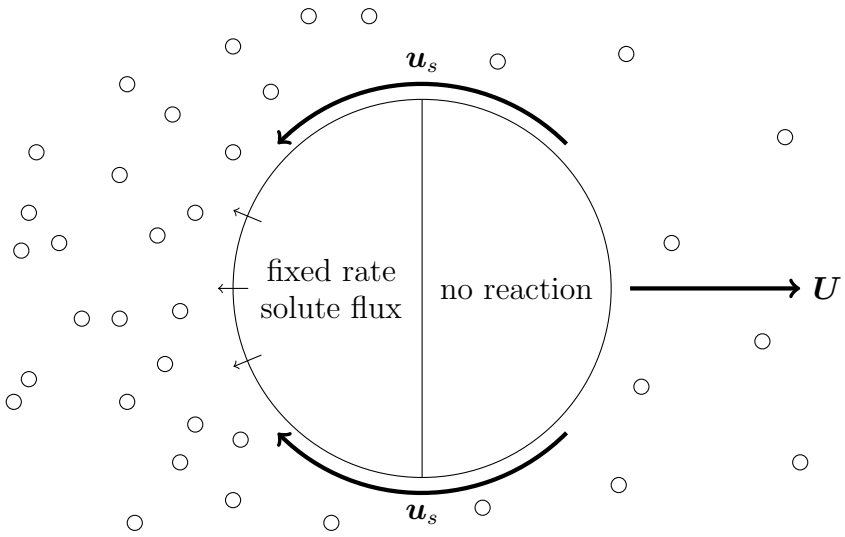

Figure 1: The process of self-diffusiophoresis is illustrated for a spherical Janus particle which emits solute at a fixed rate from its left face. Solute is more concentrated on the particle's left because of the unbalanced emission. This asymmetry induces a surface velocity $\boldsymbol{u}_s$, causing the particle to move through the surrounding fluid at velocity $\boldsymbol{U}$.

2 Principles of Self-Diffusiophoresis

In this section, the concept of self-diffusiophoresis will be explained in detail. A characteristic example of the process is presented in Fig. 1, which depicts a swimmer that releases solute at a fixed rate from half of its surface. The resulting concentration gradient induces an effective slip velocity over the particle surface, causing translation. Several results to be applied in later sections are derived as follows.

First, since microswimmers exist at small scales, we will apply the work of Taylor [1] and Purcell [2] to show that inertial effects can be neglected. In doing so, we will derive the Stokes flow equations. As in Stone and Samuel [14], these equations will yield the reciprocal theorem of Stokes flow, which explicitly relates a particle's motion and the fluid velocity imposed on its surface. Finally, we follow Anderson [7] to derive the slip velocity over a particle induced by a concentration gradient at its surface.

2.1 Stokes Flow Equations

In this essay, we consider artificial swimmers at small length scales, so inertial effects are neglected as discussed by Taylor [1] and, later, Purcell [2]. The surrounding fluid is governed by the Stokes flow equations, derived in this section. We will see that the motion of any small swimmer depends only on the instantaneous velocity distribution imposed on its boundary.

General Fluid We begin by considering Newtonian, incompressible fluid of density ρ and dynamic viscosity μ. Given the velocity and pressure distributions $\boldsymbol{u}$ and p, we write the stress and rate-of-strain tensors

$$\underline{\underline{\sigma}} = -p\underline{\underline{I}} + 2\mu\underline{\underline{e}}, \qquad \underline{\underline{e}} = \frac{1}{2}\left[\boldsymbol{\nabla u} + (\boldsymbol{\nabla u})^{\mathrm{T}}\right]. \tag{2.1}$$

The stress exerted on fluid across a boundary with outward normal $\hat{\boldsymbol{n}}$ is equal to $\underline{\underline{\sigma}} \cdot \hat{\boldsymbol{n}}$. Such fluid is described by the well known Navier-Stokes equations $\boldsymbol{\nabla} \cdot \boldsymbol{u} = 0$ and

$$\rho \left(\frac{\partial \boldsymbol{u}}{\partial t} + \boldsymbol{u} \cdot \boldsymbol{\nabla} \boldsymbol{u} \right) = \boldsymbol{f} - \boldsymbol{\nabla} p + \mu \nabla^2 \boldsymbol{u}. \tag{2.2}$$

This latter relation is simply a momentum balance: the left side represents acceleration, and the right side is the sum of body forces $\boldsymbol{f}$ and surface forces $\boldsymbol{\nabla} \cdot \underline{\underline{\sigma}}$.

We use velocity and length scales U and L to non-dimensionalize (2.2), obtaining

$$\left(\frac{\rho U^2}{L} \right) \left(\frac{\partial \boldsymbol{u}}{\partial t} + \boldsymbol{u} \cdot \boldsymbol{\nabla} \boldsymbol{u} \right) = \left(\frac{\mu U}{L^2} \right) \left(\boldsymbol{f} - \boldsymbol{\nabla} p + \nabla^2 \boldsymbol{u} \right), \tag{2.3}$$

where $\mu U/L$ has served as a pressure scale and L/U as a time scale. The bracketed numbers on the left and right sides of (2.3) are typical scales for the inertial and viscous forces in the fluid. Their ratio, the Reynolds number, is

$$\mathrm{Re} := \frac{\text{strength of inertial forces}}{\text{strength of viscous forces}} = \frac{\rho U L}{\mu}. \tag{2.4}$$

Small Length Scales The Reynolds number satisfies $\mathrm{Re} \ll 1$ at small length scales, indicating inertial forces are completely dominated by viscous forces. In that case, we neglect the left side of (2.2) to obtain the Stokes flow equations $\boldsymbol{\nabla} \cdot \boldsymbol{u} = 0$ and

$$\boxed{\mu \nabla^2 \boldsymbol{u} = \boldsymbol{\nabla} p - \boldsymbol{f}.} \tag{2.5}$$

In Stokes flow, the fluid and any submerged particles are always in quasi-static equilibrium, since there are no time derivatives in (2.5). Particle motion is completely determined by the Stokes flow equations and imposed surface velocity distribution.

2.2 Reciprocal Theorem of Stokes Flow

In this section, we follow the work of Stone and Samuel [14] to derive the reciprocal theorem of Stokes flow. We use this result to relate a particle's imposed boundary velocity distribution $\boldsymbol{u}_s$ to the corresponding swimming velocities $\boldsymbol{U}$ and $\boldsymbol{\Omega}$.

Derivation We consider two hypothetical Stokes flows $\boldsymbol{u}_1$ and $\boldsymbol{u}_2$, describing the motion of fluid which has viscosity μ and occupies some volume V, enclosed by the surface S. We introduce the quantity $2\mu \underline{\underline{e_1}} : \underline{\underline{e_2}}$, where $\underline{\underline{e_k}}$ is the rate-of-strain tensor associated with $\boldsymbol{u}_k$, and integrate this value throughout the fluid domain. After finding

$$2\mu \int_V \underline{\underline{e_1}} : \underline{\underline{e_2}} \; dV = \int_S \boldsymbol{u}_2 \cdot \underline{\underline{\sigma_1}} \cdot \hat{\boldsymbol{n}} \; dS + \int_V \boldsymbol{u}_2 \cdot \boldsymbol{f}_1 \; dV, \tag{2.6}$$

we note that the integrand's value is unchanged by swapping the indices 1 and 2. Applying the switch to the right side of (2.6) yields the reciprocal theorem,

$$\boxed{\int_S \boldsymbol{u}_1 \cdot \underline{\underline{\sigma_2}} \cdot \hat{\boldsymbol{n}} \; dS + \int_V \boldsymbol{u}_1 \cdot \boldsymbol{f}_2 \; dV = \int_S \boldsymbol{u}_2 \cdot \underline{\underline{\sigma_1}} \cdot \hat{\boldsymbol{n}} \; dS + \int_V \boldsymbol{u}_2 \cdot \boldsymbol{f}_1 \; dV.} \tag{2.7}$$

Velocity Calculation Now, we find the motion induced by an imposed boundary velocity distribution. Note that, in the preceding derivation, the unit normal $\hat{\boldsymbol{n}}$ was assumed to point out of the fluid. We adopt this convention until stating otherwise.

Consider a particle with boundary S, and let $\boldsymbol{u}_1$ and $\boldsymbol{u}_2$ be two possible Stokes flows around it. We assume both are free of body forces so that $\boldsymbol{f}_1 = \boldsymbol{f}_2 = \boldsymbol{0}$.

First Flow Assume the particle induces the boundary velocity distribution $\boldsymbol{u}_s$ in its own frame of reference, and that no outside force acts on the particle so that no net force or moment is applied to the particle by the fluid. If we denote the particle velocity $\boldsymbol{U}$ and angular velocity $\boldsymbol{\Omega}$, then the resulting global flow $\boldsymbol{u}_1$ satisfies

$$\boldsymbol{u}_1(\boldsymbol{r})\big|_{\boldsymbol{r}\in S} = \boldsymbol{U} + \boldsymbol{\Omega}\times\boldsymbol{r} + \boldsymbol{u}_s, \qquad \boldsymbol{0} = \int_S \underline{\underline{\sigma_1}}\cdot\hat{\boldsymbol{n}}\, dS, \qquad \boldsymbol{0} = \int_S \boldsymbol{r}\times\left(\underline{\underline{\sigma_1}}\cdot\hat{\boldsymbol{n}}\right) dS, \tag{2.8}$$

where $\boldsymbol{r}$ is the position vector originating at the particle center of mass.

Second Flow Assume the particle is being towed by the external force $\boldsymbol{F}'$ and moment $\boldsymbol{M}'$, so that it translates at $\boldsymbol{U}'$ and rotates with $\boldsymbol{\Omega}'$. Since Stokes flows are quasi-static, the particle experiences a drag force $-\boldsymbol{F}'$ and moment $-\boldsymbol{M}'$ exerted by the fluid. If we impose a no-slip condition on the particle, then the global flow $\boldsymbol{u}_2$ satisfies

$$\boldsymbol{u}_2(\boldsymbol{r})\Big|_{\boldsymbol{r}\in S} = \boldsymbol{U}' + \boldsymbol{\Omega}'\times\boldsymbol{r}, \qquad \boldsymbol{F}' = \int_S \underline{\underline{\sigma_2}}\cdot\hat{\boldsymbol{n}}\, dS, \qquad \boldsymbol{M}' = \int_S \boldsymbol{r}\times\left(\underline{\underline{\sigma_2}}\cdot\hat{\boldsymbol{n}}\right) dS. \tag{2.9}$$

Theorem Application Applying the reciprocal theorem (2.7) yields

$$\boldsymbol{U}\cdot\boldsymbol{F}' + \boldsymbol{\Omega}\cdot\boldsymbol{M}' = -\int_S \boldsymbol{u}_s\cdot\underline{\underline{\sigma_2}}\cdot\hat{\boldsymbol{n}}\, dS. \tag{2.10}$$

In the case of a spherical particle of radius R, it is known that the second flow satisfies

$$\underline{\underline{\sigma_2}}\cdot\hat{\boldsymbol{n}} = \frac{\boldsymbol{F}'}{4\pi R^2} + \frac{3\left(\boldsymbol{M}'\times\boldsymbol{r}\right)}{8\pi R^4}. \tag{2.11}$$

Applying this to (2.10) yields the relation

$$\boldsymbol{F}'\cdot\left[\boldsymbol{U} + \frac{1}{4\pi R^2}\int_S \boldsymbol{u}_s\, dS\right] + \boldsymbol{M}'\cdot\left[\boldsymbol{\Omega} + \frac{3}{8\pi R^4}\int_S \boldsymbol{r}\cdot\boldsymbol{u}_s\, dS\right] = 0. \tag{2.12}$$

Since this expression is true for arbitrary $\boldsymbol{F}'$ and $\boldsymbol{M}'$, the bracketed quantities must be zero. A sphere with outward normal $\hat{\boldsymbol{n}}$ and the boundary velocity $\boldsymbol{u}_s$ must swim with

$$\boxed{\boldsymbol{U} = -\frac{1}{4\pi R^2}\int_S \boldsymbol{u}_s\, dS, \qquad \boldsymbol{\Omega} = -\frac{3}{8\pi R^3}\int_S \hat{\boldsymbol{n}}\times\boldsymbol{u}_s\, dS.} \tag{2.13}$$

Two Dimensions In two dimensions, the well known "Stokes paradox" states that the dragging flow $\boldsymbol{u}_2$ does not die off at infinity, instead diverging at $\mathcal{O}\left(\log|\boldsymbol{r}|\right)$. This is concerning, but it is shown by Squires and Bazant [15] that the reciprocal theorem can be applied just as in the previous section. While the dragging flow is unphysical, it nonetheless satisfies the Stokes equations so that the analysis is valid.

With this conclusion, we calculate the swimming speed of a circular particle. The analysis is the same as in the previous section, except that we let $\boldsymbol{M}' = 0$ and the dragging flow satisfies $\underline{\underline{\sigma_2}} = \boldsymbol{F}'/2\pi R$. Since the first flow is force-free, it dies off at infinity, and only integrals on the particle surface contribute. This yields the velocity

$$\boxed{\boldsymbol{U} = -\frac{1}{2\pi}\int_0^{2\pi} \boldsymbol{u}_s \, d\theta,} \tag{2.14}$$

where θ parametrizes the particle boundary.

We have derived the relationship between a particle's motion and the velocity distribution on its surface. In the next section, we will show how such boundary velocities are induced by gradients in the solute distribution around the particle.

2.3 Gradient-Induced Slip Velocities

Janus particles swim by catalytically reacting with fluid in an asymmetric way, so that gradients are produced in the surrounding solute concentration. This process induces a tangential slip velocity over the particle surface, resulting in self-propulsion. In this section, we find an explicit representation for the boundary velocity given the bulk concentration distribution, as outlined by Anderson [7].

Geometry Consider a small, rigid particle of length scale R surrounded by solute of varying concentration c. We divide the fluid into two regions. The "inner region" is a boundary layer of thickness δ satisfying the no-slip condition on the particle's surface. The "outer region" comprises the rest of the fluid. We examine the inner region first.

Inner Region We assume the boundary layer is thin compared to the particle, so that $\delta \ll R$. As we investigate the inner region, we approximate the particle surface as planar.

Concentration Distribution Let $\hat{\boldsymbol{z}}$ denote the direction normal to the particle's surface. The solute experiences a combination of dipole and van der Waals forces and excluded volume effects, which are represented by the potential energy $\Phi(z)$, such that the expected force on individual solute molecules is $\langle \boldsymbol{F}_{\text{mol}} \rangle = -\Phi'(z)\hat{\boldsymbol{z}}$. The vertical variation of the solute concentration is described by the Boltzmann distribution

$$c(x, y, z) = c_s(x, y)e^{-\Phi(z)/kT}, \tag{2.15}$$

where c_s is the concentration on the outer edge of the boundary layer, $z \to \infty$.

Momentum Balance The mean molecular force transmits to the fluid as a body force $\boldsymbol{f} = -c\,\langle \boldsymbol{F}_{\text{mol}} \rangle$. Since both length scales δ, R are small, we obtain

$$\boldsymbol{\nabla} p + c\ \Phi'(z)\hat{\boldsymbol{z}} = \mu \nabla^2 \boldsymbol{u} \tag{2.16}$$

from the Stokes flow equations (2.5). Without loss of generality, we choose for the horizontal component of $\boldsymbol{u}$ to lie along $\hat{\boldsymbol{x}}$, so that we may omit consideration of u_y.

Scalings Since the boundary layer is thin, we assume derivatives there scale as

$$\frac{\partial}{\partial x} \sim \frac{1}{R} \ll \frac{1}{\delta} \sim \frac{\partial}{\partial z}, \tag{2.17}$$

which suggests that we can approximate the Laplacian as $\nabla^2 \approx \partial^2/\partial z^2$. We find the relative scaling of the velocity components by applying this relation to incompressibility, indicating $u_z/\delta \sim u_x/R$, and examine the vertical and horizontal components of (2.16).

The horizontal momentum balance indicates that the pressure scales as

$$p \sim \frac{\mu u_x}{\delta}\left(\frac{R}{\delta}\right) \sim \frac{\mu u_z}{\delta}\left(\frac{R}{\delta}\right)^2. \tag{2.18}$$

This immediately shows the vertical component of viscous force to be much smaller than the vertical pressure gradient, as

$$\frac{p}{\delta} \gg \frac{\mu u_z}{\delta^2}. \tag{2.19}$$

The dominant vertical balance is therefore between the pressure gradient and solute/particle interaction body force. This gives the vertical and horizontal relations

$$\frac{\partial p}{\partial z} + c\frac{d\Phi}{dz} = 0, \qquad \frac{\partial p}{\partial x} - \mu\frac{\partial^2 u_x}{\partial z^2} = 0, \tag{2.20}$$

which can be solved to find the flow within the interfacial boundary layer.

Interfacial Flow We combine (2.15) and the vertical part of (2.20) to obtain the pressure distribution

$$p = c_s(x,y)kT\ e^{-\Phi(z)/kT}. \tag{2.21}$$

We substitute this into the horizontal part to find the velocity distribution which satisfies the no-slip condition at $z = 0$,

$$\boldsymbol{u}_h(z) = \left[-\frac{kT}{\mu}\int_0^z z'\left(e^{-\Phi(z')/kT} - 1\right)dz'\right]\boldsymbol{\nabla}_{2D}c_s, \tag{2.22}$$

where we have allowed the velocity to point anywhere in the $\hat{\boldsymbol{x}}$-$\hat{\boldsymbol{y}}$ plane. The flow at the interface between the regions is given by $\lim_{z\to\infty}\boldsymbol{u}_h(z)$.

Outer Region Now, we turn our attention to the outer region. Since $\delta \ll R$, we make the approximation that the inner region is infinitesimally thin, and the interfacial velocity above exists directly on the particle surface as a tangential slip velocity $\boldsymbol{u}_s$.

Slip Velocity We express the slip velocity $\boldsymbol{u}_s = \lim_{z\to\infty}\boldsymbol{u}_h(z)$ from the perspective of the outer region by noting that, on the particle boundary with outward normal $\hat{\boldsymbol{n}}$, the planar gradient in (2.22) is given by $\boldsymbol{\nabla}_{2D}c_s = \left(\underline{\underline{I}} - \hat{\boldsymbol{n}}\hat{\boldsymbol{n}}\right)\cdot\boldsymbol{\nabla}c$. In addition, the bracketed quantity depends on environmental factors such as temperature, viscosity, and details of the solute/particle force. For ease of notation, we define the "surface mobility"

$$\boxed{M := -\frac{kT}{\mu}\int_0^\infty z\left(e^{-\Phi(z)/kT} - 1\right)dz,} \tag{2.23}$$

and write the slip velocity in the form

$$\boxed{\boldsymbol{u}_s = M\left(\underline{\underline{I}} - \hat{\boldsymbol{n}}\hat{\boldsymbol{n}}\right)\cdot\boldsymbol{\nabla}c.} \tag{2.24}$$

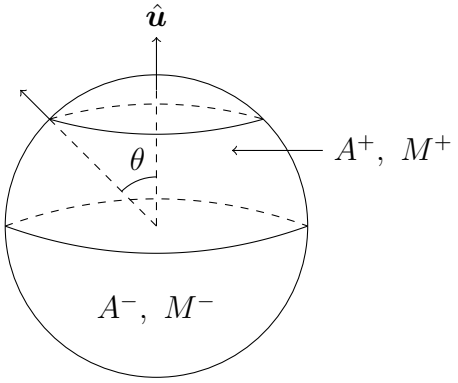

Figure 2: A Janus particle with symmetry axis $\hat{\boldsymbol{u}}$. The surface activity and mobility A and M depend only on the polar angle θ. On the upper hemisphere, they are equal to the constant values A^+ and M^+. On the lower hemisphere, they are A^- and M^-.

Concentration Distribution Finally, we consider the evolution of solute in the bulk as outlined by Golestanian et al. [6], which takes the form

$$\frac{\partial c}{\partial t} + \boldsymbol{u} \cdot \boldsymbol{\nabla} c = D \nabla^2 c. \tag{2.25}$$

We non-dimensionalize with velocity, concentration and length scales U, C and L to find

$$\left(\frac{UC}{L}\right)\left(\frac{\partial c}{\partial t} + \boldsymbol{u} \cdot \boldsymbol{\nabla} c\right) = \left(\frac{DC}{L^2}\right)\nabla^2 c, \tag{2.26}$$

where L/U has served as a time scale. The bracketed numbers on the left and right are scales for advective and diffusive solute transport rates; their ratio, the Péclet number, is

$$\mathrm{Pe} := \frac{\text{advective transport rates}}{\text{diffusive transport rates}} = \frac{UL}{D}. \tag{2.27}$$

For the remainder of this essay, we assume $\mathrm{Pe} \ll 1$ and neglect the left side of (2.25). In that case, the concentration distribution is harmonic, and the solute is in quasi-static equilibrium, like the surrounding fluid. We complete the analysis by defining the "surface activity" A, which measures the rate of emission or absorption of solute per unit area on a boundary. With this boundary condition, the solute distribution is determined by

$$\nabla^2 c = 0, \quad \hat{\boldsymbol{n}} \cdot \boldsymbol{\nabla} c = -\frac{A}{D}, \tag{2.28}$$

where positive values of A correspond to the emission of solute. For simplicity, we assume that A at each point on the particle surface is constant.

Using this notation, we define Janus particles more explicitly. Consider a sphere which has axisymmetric activity and mobility distributions A and M on its surface. If the activity distribution A is not symmetric above and below the equator, the solute emission is two-faced and the sphere is a Janus particle. Examples are shown in Fig. 2, where A and M are constant on each hemisphere, and Fig. 1, where A is positive and zero on the left and right hemispheres, respectively. We extend the definition to circular particles in two-dimensional environments.

3 Case Studies, Three Dimensions

In the following case studies, we will explicitly relate a Janus particle's activity and mobility distributions A and M to its motion through unbounded fluid by applying the relations derived in the preceding section. We will also investigate the general effects of confinement by considering a Janus swimmer near an infinite planar wall.

First, in this section, we will consider the three-dimensional case of a spherical Janus particle. The exact solution to the swimmer in unbounded fluid will be outlined by Golestanian et al. [6], and we will consider an approximate treatment for the swimmer near a wall developed by Ibrahim and Liverpool [13]. While the approximation will shed light on some confinement effects, it will be unable to explain certain behavior observed in numerical simulations by Uspal, Popescu, Dietrich and Tasinkevych [4].

In the following section, we will consider the two-dimensional case of a circular particle. We will see that both the unbounded and confined cases can be solved exactly using a complex approach employed by Crowdy [10]. Using this method, the solution will be attained for a more general particle configuration, revealing indirect evidence for the observed numerical behavior.

3.1 Unbounded Fluid

This section reproduces the work of Golestanian et al. [6] to calculate the swimming speed of a spherical Janus particle in unbounded fluid. Let the boundary of the particle be S, and let its radius R be small so that the Stokes flow equations apply. Given the surface activity and mobility distributions A and M, we solve Laplace's equation to find the bulk concentration distribution c at zero Péclet number, fixing the slip velocity $\boldsymbol{u}_s$ and particle swimming speed U. The relevant conclusions from the previous section are

$$\boldsymbol{U} = -\frac{1}{4\pi R^2}\int_S \boldsymbol{u}_s \, dS, \qquad \boldsymbol{\Omega} = -\frac{3}{8\pi R^3}\int_S \hat{\boldsymbol{n}} \times \boldsymbol{u}_s \, dS, \tag{2.13}$$

$$\boldsymbol{u}_s = M\left(\underline{\underline{I}} - \hat{\boldsymbol{n}}\hat{\boldsymbol{n}}\right)\cdot \boldsymbol{\nabla} c, \tag{2.24}$$

$$\nabla^2 c = 0, \quad \hat{\boldsymbol{n}}\cdot\boldsymbol{\nabla} c = -\frac{A}{D}. \tag{2.28}$$

Note that, for activity and mobility scales A' and M', the swimming speed scales as $U \sim A'M'/D$ and is independent of particle size. This is a consequence of the fixed-flux boundary condition and is not generally true in physical systems, where A can depend on the local and global distribution of fuel sources.

General Configurations Let the particle symmetry axis $\hat{\boldsymbol{u}} = \hat{\boldsymbol{z}}$ so that θ is the polar angle of spherical coordinates, as shown in Fig. 2. We write the activity and mobility distributions in terms of the Legendre polynomials,

$$A(\theta) = \sum_{k=0}^{\infty} A_k P_k(\cos\theta), \qquad M(\theta) = \sum_{k=0}^{\infty} M_k P_k(\cos\theta). \tag{3.1}$$

Note that the surface geometry of the particle is completely determined by $\{A_k\}$, $\{M_k\}$. Given these coefficients, we solve (2.28) to obtain the concentration distribution

$$c = c_0 + \frac{R}{D}\sum_{k=0}^{\infty} \frac{A_k}{k+1}\left(\frac{R}{r}\right)^{k+1} P_k(\cos\theta). \tag{3.2}$$

Since this relation depends only on r and θ, we compute the tangential portion of its gradient using the polar component of the gradient operator in spherical coordinates,

$$(\underline{\underline{I}} - \hat{\boldsymbol{n}}\hat{\boldsymbol{n}}) \cdot \boldsymbol{\nabla} c\Big|_{r=R} = \frac{\hat{\boldsymbol{\theta}}}{r}\frac{\partial c}{\partial \theta}\Big|_{r=R} = -\frac{\hat{\boldsymbol{\theta}}}{D\sin\theta}\sum_{k=0}^{\infty} A_k \left[\cos\theta P_k(\cos\theta) - P_{k+1}(\cos\theta)\right]. \quad (3.3)$$

Substituting this value into (2.24), and applying the recurrence relation

$$(2k+1)\zeta P_k(\zeta) = (k+1)P_{k+1}(\zeta) + kP_{k-1}(\zeta), \quad (3.4)$$

returns the tangential slip velocity

$$\boldsymbol{u}_s = -\frac{\hat{\boldsymbol{\theta}}}{D\sin\theta}\sum_{k=0}^{\infty}\sum_{l=0}^{\infty} A_k M_l \left(\frac{k}{2k+1}\right)\left[P_{k-1}(\cos\theta)P_l(\cos\theta) - P_{k+1}(\cos\theta)P_l(\cos\theta)\right] \quad (3.5)$$

The motion of the particle is given by (2.13), but $\boldsymbol{\Omega} = 0$ due to azimuthal symmetry. For the same reason, when we calculate the velocity by integrating (3.5) over the sphere's surface, only the vertical portion of the integral contributes, yielding

$$\boldsymbol{U} = -\frac{\hat{\boldsymbol{z}}}{2}\int_0^{\pi} (\boldsymbol{u}_s \cdot \hat{\boldsymbol{z}})\sin\theta \; d\theta. \quad (3.6)$$

After applying $\hat{\boldsymbol{\theta}} \cdot \hat{\boldsymbol{z}} = -\sin\theta$, and the orthogonality relation

$$\int_{-1}^{1} P_n(\zeta)P_m(\zeta)d\zeta = \left(\frac{2}{2n+1}\right)\delta_{nm}, \quad (3.7)$$

the swimming speed simplifies to

$$\boxed{\boldsymbol{U} = -\frac{\hat{\boldsymbol{z}}}{D}\sum_{k=0}^{\infty}\left(\frac{k+1}{2k+3}\right)A_{k+1}\left[\frac{M_k}{2k+1} - \frac{M_{k+2}}{2k+5}\right].} \quad (3.8)$$

This is the explicit dependence of the particle swimming speed on the surface patterning, expressed in the coefficients $\{A_k\}$ and $\{M_k\}$.

Two Hemispheres Configuration The most important case of surface patterning to investigate is the two hemispheres configuration pictured in Figs. 1 and 2, where A and M are constant on each half of the sphere so that

$$A(\theta) = \begin{cases} A^+, & 0 < \theta < \pi/2 \\ A^-, & \pi/2 < \theta < \pi \end{cases}, \qquad M(\theta) = \begin{cases} M^+, & 0 < \theta < \pi/2 \\ M^-, & \pi/2 < \theta < \pi \end{cases}. \quad (3.9)$$

Recall that this design can be fabricated using current manufacturing techniques, in which one or both hemispheres are coated in materials of varying catalytic properties [8].

We compute the swimming speed by introducing $\zeta = \cos\theta$ and writing

$$A(\zeta) = A^- + \left(A^+ - A^-\right)H(\zeta), \qquad M(\zeta) = M^- + \left(M^+ - M^-\right)H(\zeta), \quad (3.10)$$

where $H(\zeta)$ is the Heaviside step function. Consider the decomposition of $H(\zeta)$ into the Legendre coefficients $\{H_k\}$. Given the shape of the function, $H_0 = 1/2$ must be the only

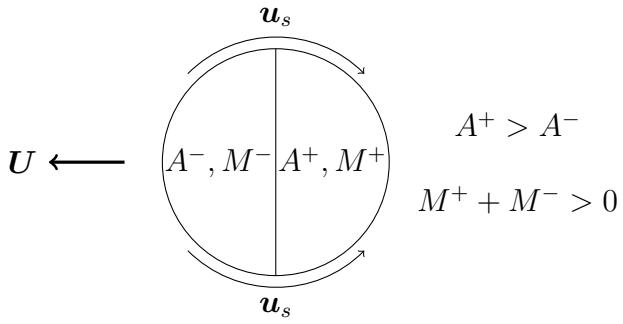

Figure 3: A Janus swimmer with positive mobility swims away from the hemisphere with higher surface activity, as shown above. A swimmer with negative mobility does the opposite, swimming towards the source hemisphere (not shown).

non-zero even coefficient. Every even A_k and M_k with $k > 0$ must be zero as well. This implies the $k = 0$ term in (3.8) is the only contributor to the swimming speed, yielding

$$\boldsymbol{U} = -\frac{M_0 A_1 \hat{\boldsymbol{z}}}{3D}. \tag{3.11}$$

Since the Legendre polynomials are orthogonal as in (3.7), we apply

$$f_k = \frac{2k+1}{2} \int_{-1}^{1} f(\zeta) P_k(\zeta) d\zeta, \tag{3.12}$$

to determine the coefficients

$$M_0 = \frac{M^+ + M^-}{2}, \qquad A_1 = \frac{3}{4}\left(A^+ - A^-\right), \tag{3.13}$$

and the two-hemispheres swimming speed

$$\boxed{\boldsymbol{U} = \frac{\hat{\boldsymbol{z}}}{8D}\left(M^- + M^+\right)\left(A^- - A^+\right).} \tag{3.14}$$

Discussion

Swim Direction For positive average mobility, the particle tends to swim in the opposite direction of the hemisphere with higher activity, as shown in Fig. 3 and, earlier, Fig. 1. The reverse is true if the average mobility is negative. For the remainder of the essay, when referring to the "nose" or "tail" of a particle, we do so under the assumption of positive mobility unless specifically noted otherwise.

Solute Source vs. Dipole Effects The swimming speed scales with A_1, which quantifies the difference in activity between the two hemispheres, not the average activity A_0. Eq. 3.2 shows that, in the multipole expansion of the concentration distribution, A_0 and A_1 measure the strengths of the $\mathcal{O}(r^{-1})$ source and $\mathcal{O}(r^{-2})$ dipole terms, respectively.

In the special case where $A_0 = 0$, the source term vanishes and the dipole function becomes leading-order. For identical A_1, this recovers the same $\boldsymbol{U}$ as a particle with nonzero A_0, despite a qualitative difference in their concentration far-fields. We conclude

that the unbounded swim speed does not depend on whether an unbounded particle is a net source of solute. This is not the case near a wall, where the solute far-field interacts with the confining geometry. This is explicitly shown in the next section, as Ibrahim and Liverpool [13] show the dominant wall effect on Janus swimmers scales with A_0, not A_1.

Approximations to Surface Geometry General distributions of A and M can be replaced with approximations to simplify the resulting solute distribution and global flows. The two-hemispheres model is approximated by the linear activity function

$$A(\zeta) = \left(\frac{A^+ + A^-}{2}\right) + \frac{3}{4}\left(A^+ - A^-\right)\zeta, \tag{3.15}$$

which yields the correct swimming speed (3.14). It follows from (3.2) that the approximate bulk concentration distribution is accurate to $\mathcal{O}(r^{-2})$ and terminates after two terms; this is much simpler to work with than the true distribution function, which is an infinite series. Unfortunately, the slip velocity (3.5) remains an infinite series.

Studying particles with constant mobility avoids this problem. For $M = M_0$, any activity pattern $\{A_k\}$ can be approximated by the function $A(\zeta) = A_0 + A_1\zeta$ to obtain the correct swim speed and convenient, two-term representations of the concentration and slip velocity. Ibrahim and Liverpool [13] use this approach in the next section.

3.2 Near Infinite Wall

In this section, we apply an approximation developed by Ibrahim and Liverpool [13] to find the leading-order effects of a planar wall on the motion of a nearby Janus particle. After introducing the unbounded solution from the previous section, we add image singularity systems at unphysical locations to satisfy boundary conditions on the wall and swimmer surface. The values of the image systems evaluated on the particle boundary can be translated into velocity and rotation corrections through the reciprocal theorem.

Surface Geometry Consider a particle of the two-hemispheres configuration with constant mobility $M^+ = M^- = M_0$ and one inert face, so that $A^+ = 0$ as in Fig. 1. As discussed, the solute concentration and surrounding flow are greatly simplified by approximating the piecewise activity distribution with the linear function $A(\zeta) = A_0 + A_1\zeta$.

If we allow the particle symmetry axis $\hat{\boldsymbol{u}}$ to vary, then the unbounded solute distribution, slip velocity and swim speed are given by (3.2), (3.5) and (3.8) to be

$$\boxed{c^{(0)} = c_0 + \frac{A_0 R}{D}\left(\frac{R}{r}\right) + \frac{A_1 R}{2D}\left(\frac{R}{r}\right)^2 \hat{\boldsymbol{u}}\cdot\hat{\boldsymbol{r}},} \tag{3.16}$$

$$\boldsymbol{u}_s^{(0)} = \frac{M_0 A_1}{2D}\left(\underline{\underline{I}} - \hat{\boldsymbol{n}}\hat{\boldsymbol{n}}\right)\cdot\hat{\boldsymbol{u}}, \tag{3.17}$$

$$\boxed{\boldsymbol{U}_0 = -\frac{M_0 A_1}{3D}\hat{\boldsymbol{u}},} \tag{3.18}$$

where $\hat{\boldsymbol{n}}$ is the particle's outward normal. After noting $\boldsymbol{u}^{(0)} = \boldsymbol{U} + \boldsymbol{u}_s$ on $r = R$, we solve the Stokes flow equations to find the bulk flow

$$\boxed{\boldsymbol{u}^{(0)} = \frac{M_0 A_1}{6D}\left(\frac{\underline{\underline{I}}}{r^3} - \frac{3\boldsymbol{r}\boldsymbol{r}}{r^5}\right)\cdot\hat{\boldsymbol{u}}.} \tag{3.19}$$

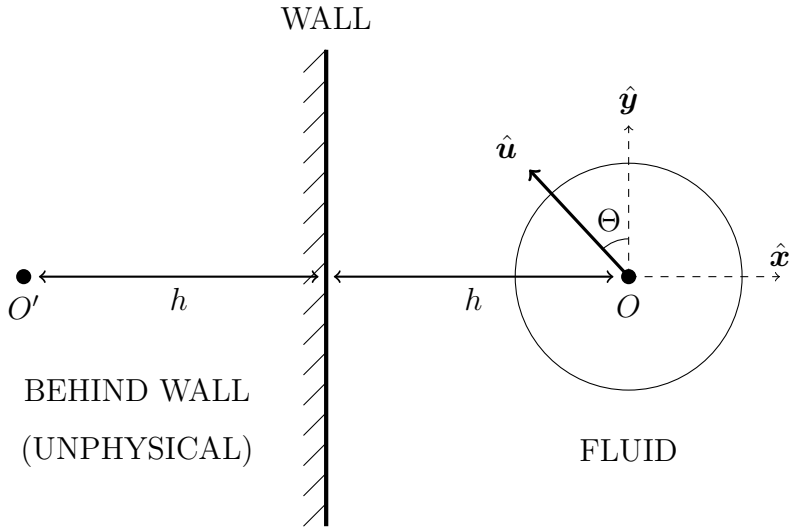

Figure 4: The particle sits at a distance h from the wall, and the tilt angle between its symmetry axis $\hat{\boldsymbol{u}}$ and $\hat{\boldsymbol{y}}$ is Θ. During the analysis, the image solute and velocity systems $c^{(1)}$ and $\boldsymbol{u}^{(1)}$ are placed at the unphysical position O' ($x = -2h$) to satisfy boundary conditions on the wall. Similarly, the image systems $c^{(2)}$ and $\boldsymbol{u}^{(2)}$ are placed at the particle center O ($x = y = 0$) to satisfy the boundary conditions on the particle surface.

We assume $M_0 A_1 < 1$ so that $\boldsymbol{U}_0$ lies along $\hat{\boldsymbol{u}}$. In keeping with our assumption of positive mobility, $A_1 < 1$ and the inert face acts as the nose of the particle.

Wall Geometry The geometry of the problem is illustrated in Fig. 4. Fixing the origin at the particle center as before, we let the wall lie parallel to the $\hat{\boldsymbol{y}}$ axis on the line $x = -h$. Denoting Θ as the tilt angle between the symmetry axis $\hat{\boldsymbol{u}}$ and $\hat{\boldsymbol{y}}$, we decompose $\hat{\boldsymbol{u}}$ into component vectors $\hat{\boldsymbol{u}}^{\parallel} = \cos\Theta\ \hat{\boldsymbol{y}}$ and $\hat{\boldsymbol{u}}^{\perp} = -\sin\Theta\ \hat{\boldsymbol{x}}$. Finally, we introduce the parameter $\varepsilon = R/h$, such that $\varepsilon \ll 1$ when the particle is far from the wall.

Image Systems We introduce concentration and velocity singularity systems at the unphysical locations $x = -2h$ (the particle's mirror image across the wall) and $x = y = 0$ (the particle center), to satisfy boundary conditions on the wall and particle surface. On the wall, these are no solute flux and no fluid slip; on the particle, they are no fluid flux and the fixed-flux solute condition from (2.28).

Solute Distributions We satisfy the no-flux solute condition on the wall by introducing the mirror image of the unbounded concentration distribution across the wall,

$$\boxed{c^{(1)} = \frac{A_0 R}{D}\left(\frac{R}{r'}\right) + \frac{A_1 R}{2D}\left(\frac{R}{r'}\right)^2 \left(\hat{\boldsymbol{u}}^{\parallel} - \hat{\boldsymbol{u}}^{\perp}\right) \cdot \hat{\boldsymbol{r}}',} \tag{3.20}$$

where $\boldsymbol{r}' = \boldsymbol{r} + 2h\hat{\boldsymbol{x}}$ is the position vector from the image location. The sum $c^{(0)} + c^{(1)}$ is exactly symmetric about the wall, so there is no normal gradient and no solute flux.

By introducing $c^{(1)}$, we have violated the fixed-flux boundary condition on the swimmer. Taylor expanding about the particle center gives the normal gradient of the image

solute to be $\hat{\boldsymbol{n}} \cdot \boldsymbol{\nabla} c_1 = \hat{\boldsymbol{n}} \cdot \boldsymbol{\nabla} c_1(\boldsymbol{0}) + \mathcal{O}(\varepsilon^4)$, and we calculate

$$\boldsymbol{\nabla} c^{(1)}(\boldsymbol{0}) = \frac{A_0}{16D}\left[-4\varepsilon^2 \hat{\boldsymbol{x}} + \frac{A_1 \varepsilon^3}{A_0}\left(2\hat{\boldsymbol{u}}^{\perp} + \hat{\boldsymbol{u}}^{\parallel}\right)\right]. \tag{3.21}$$

To satisfy the fixed-flux boundary condition, we introduce the second image system $c^{(2)}$ at the particle center, such that $\hat{\boldsymbol{n}} \cdot \boldsymbol{\nabla} c^{(1)} = -\hat{\boldsymbol{n}} \cdot \boldsymbol{\nabla} c^{(2)}$. This is satisfied by

$$\boxed{c^{(2)} = \frac{A_0 R}{32D}\left(\frac{R}{r}\right)^2 \left[-4\varepsilon^2 \hat{\boldsymbol{x}} + \frac{A_1 \varepsilon^3}{A_0}\left(2\hat{\boldsymbol{u}}^{\perp} + \hat{\boldsymbol{u}}^{\parallel}\right)\right] \cdot \hat{\boldsymbol{r}}.} \tag{3.22}$$

By introducing $c^{(2)}$, we have again violated the no flux condition on the wall. While this process can be repeated to find the concentration as a power series in ε, such that $c = c^{(0)} + c^{(1)} + c^{(2)} + \cdots$, we will stop here.

Surrounding Flows At this point, we repeat the above process for the surrounding flow. The unbounded solution $\boldsymbol{u}^{(0)}$ is a source-dipole singularity centered at the origin. Many techniques at low Reynolds number, such as slender-body theory, involve distributions of fundamental singularities. Since these analyses are often conducted near a planar wall, the corresponding image systems which satisfy the no-slip condition have been derived for many flows, as in Blake and Chwang [16]. If we define the tensors

$$\underline{\underline{G}}(\boldsymbol{r}) = R\left(\frac{\underline{\underline{I}}}{r} + \frac{\boldsymbol{r}\boldsymbol{r}}{r^3}\right), \quad \underline{\underline{D}}(\boldsymbol{r}) = \frac{R^3}{2}\left(\frac{3\boldsymbol{r}\boldsymbol{r}}{r^5} - \frac{\underline{\underline{I}}}{r^3}\right), \tag{3.23}$$

then the singularity system at $x = -2h$ which yields no fluid slip on the wall is

$$\boxed{\begin{aligned}\boldsymbol{u}^{(1)} = {} & \underline{\underline{D}}(\boldsymbol{r}') \cdot \left(\boldsymbol{U}_0^{\parallel} - 3\boldsymbol{U}^{\perp}\right) - 2h\left(\hat{\boldsymbol{x}} \cdot \boldsymbol{\nabla}\right) \underline{\underline{D}}(\boldsymbol{r}') \cdot \left(\boldsymbol{U}_0^{\parallel} - \boldsymbol{U}_0^{\perp}\right) \\ & + R^2\left(\boldsymbol{U}_0^{\parallel} \cdot \boldsymbol{\nabla}\right)\left(\hat{\boldsymbol{x}} \cdot \boldsymbol{\nabla}\right) \underline{\underline{G}}(\boldsymbol{r}') \cdot \hat{\boldsymbol{x}} - R^2\left(\hat{\boldsymbol{x}} \cdot \boldsymbol{\nabla}\right)\left(\hat{\boldsymbol{y}} \cdot \boldsymbol{\nabla}\right) \underline{\underline{G}}(\boldsymbol{r}') \cdot \boldsymbol{U}_0^{\perp},\end{aligned}} \tag{3.24}$$

where $\boldsymbol{r}' = \boldsymbol{r} + 2h\hat{\boldsymbol{x}}$ and $\boldsymbol{U}_0^{\parallel} = U_0 \cos\Theta\ \hat{\boldsymbol{y}},\ \boldsymbol{U}_0^{\perp} = -U_0 \sin\Theta\ \hat{\boldsymbol{x}}$.

As before, in introducing $\boldsymbol{u}^{(1)}$ we have violated the no fluid flux condition on the particle surface. While we nominally introduce a flow $\boldsymbol{u}^{(2)}$ centered at the particle, such that $\hat{\boldsymbol{n}} \cdot \boldsymbol{u}^{(1)} = -\hat{\boldsymbol{n}} \cdot \boldsymbol{u}^{(2)}$ on its surface, we do not need to compute a representation for the flow to calculate the effects of the collective image systems.

Velocity Corrections Given the total solute and velocity distributions

$$c = c^{(0)} + c^{(1)} + c^{(2)} + \mathcal{O}\left(\varepsilon^4\right), \qquad \boldsymbol{u} = \boldsymbol{u}^{(0)} + \boldsymbol{u}^{(1)} + \boldsymbol{u}^{(2)} + \mathcal{O}\left(\varepsilon^6\right), \tag{3.25}$$

the velocity corrections $\boldsymbol{U}_1$ and $\boldsymbol{\Omega}_1$ to the unbounded velocity $\boldsymbol{U}_0$ satisfy

$$\boldsymbol{U}_1 + \boldsymbol{\Omega}_1 \times \boldsymbol{r} = \boldsymbol{u}^{(1)} + \boldsymbol{u}^{(2)} - M_0\left(\underline{\underline{I}} - \hat{\boldsymbol{n}}\hat{\boldsymbol{n}}\right) \cdot \boldsymbol{\nabla}\left(c^{(1)} + c^{(2)}\right) \tag{3.26}$$

on the swimmer's surface. Since the particle is force-free, the force and torque exerted by $\boldsymbol{u}^{(2)}$ across $r = R$ must be zero. This is analogous to our application of the reciprocal

theorem in §2.2, using the boundary velocity distribution $\boldsymbol{u}_s = -\boldsymbol{u}^{(1)} + M_0 \boldsymbol{\nabla}_s \left(c^{(1)} + c^{(2)}\right)$, where $\boldsymbol{\nabla}_s$ is the surface gradient $\left(\underline{\underline{I}} - \hat{\boldsymbol{n}}\hat{\boldsymbol{n}}\right) \cdot \boldsymbol{\nabla}$. We apply (2.13) to obtain

$$\begin{aligned} \boldsymbol{U}_1 &= \frac{1}{4\pi R^2} \int_S \left[\boldsymbol{u}^{(1)} - M_0 \boldsymbol{\nabla}_s \left(c^{(1)} + c^{(2)}\right)\right] dS, \\ \boldsymbol{\Omega}_1 &= \frac{3}{8\pi R^3} \int_S \hat{\boldsymbol{n}} \times \left[\boldsymbol{u}^{(1)} - M_0 \boldsymbol{\nabla}_s \left(c^{(1)} + c^{(2)}\right)\right] dS. \end{aligned} \tag{3.27}$$

Note that $\boldsymbol{u}^{(1)}$ is biharmonic and $c^{(1)}$ is harmonic. Since both are non-singular at the particle center, they can be Taylor expanded to the surface, where their integrated series terminate. This yields the simplified expressions

$$\begin{aligned} \boldsymbol{U}_1 &= \boldsymbol{u}^{(1)}(\boldsymbol{0}) + \frac{R^2}{6}\nabla^2 \boldsymbol{u}^{(1)}(\boldsymbol{0}) - \frac{2M_0}{3}\boldsymbol{\nabla} c^{(1)}(\boldsymbol{0}) - \frac{M_0}{4\pi R^2}\int_S \boldsymbol{\nabla}_s c^{(2)} dS, \\ \boldsymbol{\Omega}_1 &= \frac{1}{2}\left(\boldsymbol{\nabla} \times \boldsymbol{u}^{(1)}(\boldsymbol{0})\right) - \frac{3M_0}{8\pi R^3}\int_S \boldsymbol{r} \times \boldsymbol{\nabla}_s c^{(2)} dS, \end{aligned} \tag{3.28}$$

for the leading-order corrections to the motion of a Janus particle near a planar wall.

We can explicitly separate these effects into two categories based on whether they are induced by the image solute systems (diffusiophoretic effects) or the image flows (hydrodynamic effects). Each is examined more closely below.

Diffusiophoretic Effects Wall-induced diffusiophoresis causes the corrections

$$\boldsymbol{U}_1^d = -\frac{2M_0}{3}\boldsymbol{\nabla} c^{(1)}(\boldsymbol{0}) - \frac{M_0}{4\pi R^2}\int_S \boldsymbol{\nabla}_s c^{(2)}\, dS, \tag{3.29}$$

$$\boldsymbol{\Omega}_1^d = -\frac{3M_0}{8\pi R^3}\int_S \boldsymbol{r} \times \boldsymbol{\nabla}_s c^{(2)}\, dS. \tag{3.30}$$

The surface gradient of $c^{(2)}$ in Cartesian coordinates is

$$\begin{aligned} (\underline{\underline{I}} - \hat{\boldsymbol{n}}\hat{\boldsymbol{n}}) \cdot \boldsymbol{\nabla} c^{(2)} = \frac{1}{32Dh^3R}\Big\{ &\left[-A_1 Rxy\cos\Theta + 2(y^2+z^2)(2A_0 h + A_1 R\sin\Theta)\right]\hat{\boldsymbol{x}} \\ &+ \left[A_1 R(x^2+y^2)\cos\Theta + 2xy(2A_0 h + A_1 R\sin\Theta)\right]\hat{\boldsymbol{y}} \\ &+ \left[z\left(4A_0 hx - A_1 Ry\cos\Theta + 2A_1 Rx\sin\Theta\right)\right]\hat{\boldsymbol{z}}\Big\}, \end{aligned} \tag{3.31}$$

which, when integrated over the sphere surface, yields the average value

$$\int_S \boldsymbol{\nabla}_s c^{(2)}\, dS = -\frac{A_0 R^4 \pi}{3Dh^2}\hat{\boldsymbol{x}} + \frac{A_1 R^5 \pi}{6Dh^3}\hat{\boldsymbol{u}}^{\perp} + \frac{A_1 R^5 \pi}{12Dh^3}\hat{\boldsymbol{u}}^{\parallel}. \tag{3.32}$$

Substituting (3.21) and (3.32) into (3.29) yields the diffusiophoretic velocity correction

$$\boxed{\boldsymbol{U}_1^d = \frac{M_0 A_0 \varepsilon^2}{4D}\hat{\boldsymbol{x}} + \frac{3\varepsilon^3}{16}\left(2\boldsymbol{U}_0^{\perp} + \boldsymbol{U}_0^{\parallel}\right) + \mathcal{O}(\varepsilon^4).} \tag{3.33}$$

Examining (3.31) reveals the cross product $\boldsymbol{r} \times \boldsymbol{\nabla}_s c^{(2)}$ will integrate to zero on the sphere surface. Solute effects have no impact on the particle's rotation at this order, and $\boldsymbol{\Omega}_1^d = \boldsymbol{0}$.

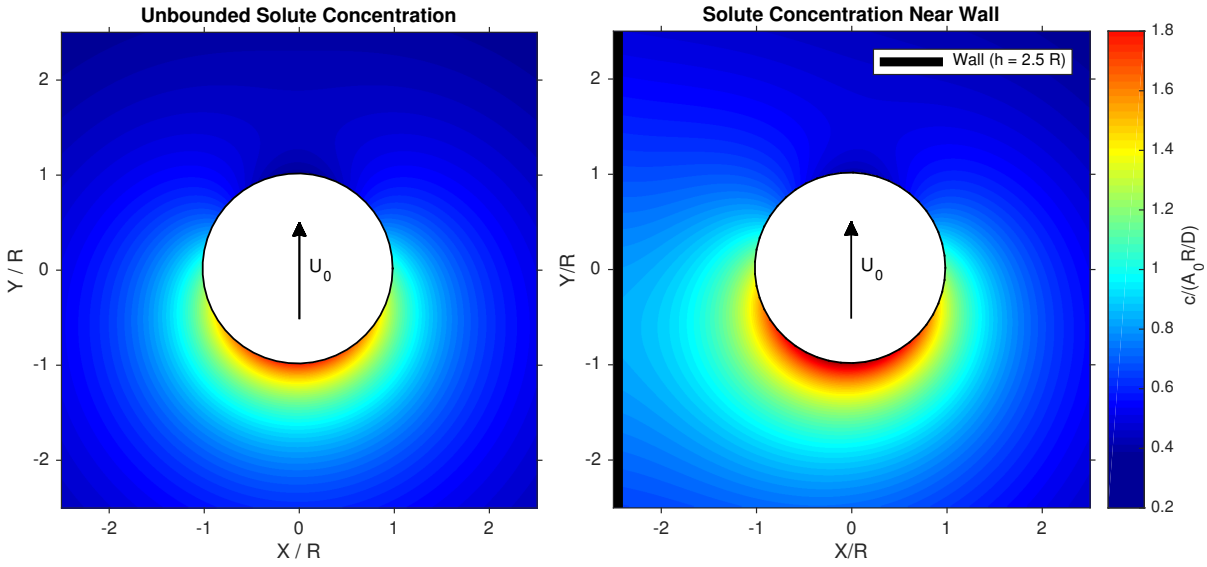

(a) (b)

Figure 5: The distribution of solute around the particle at orientation $\Theta = 0$ is shown for unbounded fluid (a) and near a wall (b). In the latter case, confinement limits the diffusion of solute from the space between the particle and the wall. The resulting build-up of solute creates a gradient which drives repulsive motion.

The dominant effect on the particle's motion is related to the source activity coefficient A_0. This demonstrates that concentration gradients can be generated purely by geometrical asymmetry, as in Michelin and Lauga [5], who explain that confinement limits solute diffusion relative to the unbounded case. Because of this, the area between the particle and the wall experiences a higher concentration than the space opposite the particle, as shown in Fig. 5. This asymmetry drives a repulsion which is independent of the particle's orientation. Subdominant effects enhance the particle's motion.

Hydrodynamic Effects Wall-induced hydrodynamic effects yield the velocities

$$\boxed{\boldsymbol{U}_1^h = -\frac{\varepsilon^3}{8D}\left(4\boldsymbol{U}^{\perp} + \boldsymbol{U}^{\parallel}\right) + \mathcal{O}(\varepsilon^6),} \tag{3.34}$$

$$\boxed{\boldsymbol{\Omega}_1^h = \frac{3\varepsilon^4}{16R}\left(\boldsymbol{U}^{\parallel} \times \boldsymbol{r}\right) + \mathcal{O}(\varepsilon^7).} \tag{3.35}$$

The hydrodynamic velocities restrict the swimmer's motion, opposing the diffusiophoretic effects at the same order. The image flow also induces a rotation of the particle. Because of symmetry, we need only consider orientations for which $\boldsymbol{U}_0 \cdot \hat{\boldsymbol{y}} \geq 0$. We find the particle always rotates away from the wall, unless $\Theta = \pm\pi/2$, where there is no rotation.

Equations of Motion At this point, we have the information required to determine the particle's time evolution near a wall. For a swimmer at $\boldsymbol{r}_0 = h\hat{\boldsymbol{x}} + y\hat{\boldsymbol{y}}$, we identify

$$\frac{d\boldsymbol{r}_0}{dt} = \boldsymbol{U}(t), \qquad \frac{d\hat{\boldsymbol{u}}}{dt} = \boldsymbol{\Omega}(t) \times \hat{\boldsymbol{u}}(t), \tag{3.36}$$

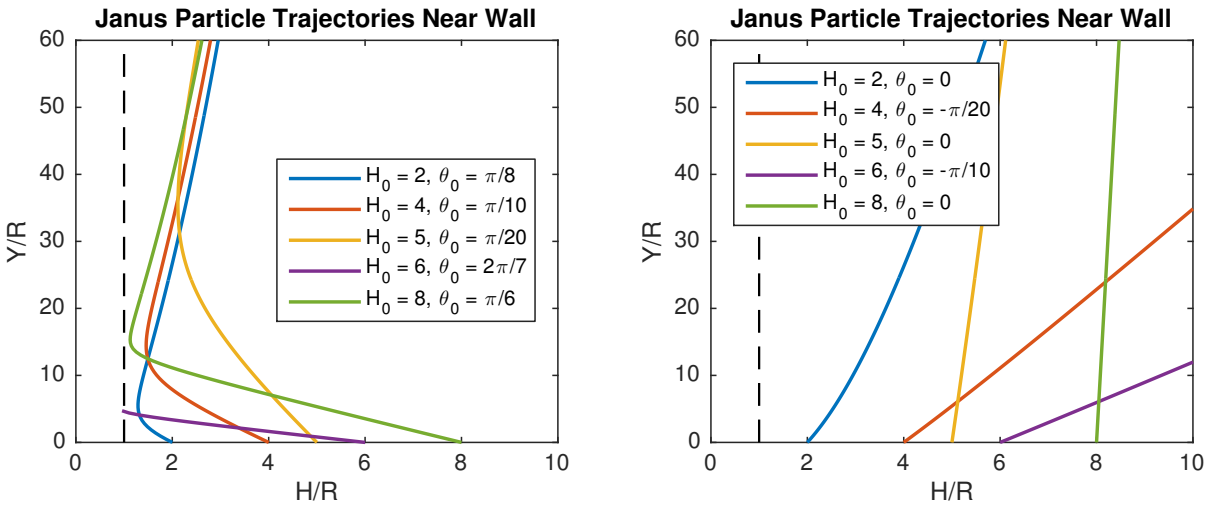

Figure 6: Numerically integrated trajectories of spherical Janus swimmers near an infinite planar wall. All trajectories begin at $Y = 0$. The activities satisfy $A_* = 1/2$ to recover the effects of an inert hemisphere swimmer. Particles in the left image are originally oriented towards the wall, while those on the right are initially parallel or oriented away.

with $\boldsymbol{U}(t) = \boldsymbol{U}_0 + \boldsymbol{U}_1^d + \boldsymbol{U}_1^h$ and $\boldsymbol{\Omega} = \boldsymbol{\Omega}_1^h$. After introducing the dimensionless quantities $H = h/R$, $Y = y/R$, $\tau = tU_0/R$, and $A_* = -3A_0/4A_1$, we obtain the following set of equations presented by Ibrahim and Liverpool [13].

$$\begin{aligned} \frac{dH}{d\tau} &= \frac{A_*}{H^2} + \left[-1 + \frac{1}{8H^3}\right] \sin\Theta, \\ \frac{dY}{d\tau} &= \left[1 + \frac{1}{16H^3}\right] \cos\Theta, \\ \frac{d\Theta}{d\tau} &= -\frac{3}{16H^4} \cos\Theta. \end{aligned} \tag{3.37}$$

The largest errors which enter the analysis are $\mathcal{O}(R^4/H^4)$, which reach $\sim$1% at $H = 3R$, $\sim$6% at $H = 2R$ and $\sim$20% at $H = 1.5R$.

Discussion

General Effects The leading-order effect on a particle is a solute-induced repulsion from the wall. At lower order, parallel motion is enhanced and normal motion is restricted. Hydrodynamic effects rotate the particle away from the wall for $|\Theta| < \pi/2$.

Particle Trajectories These equations can be numerically integrated to compute swimmer trajectories for various initial conditions, as I have done in Fig. 6. The non-dimensional source strength $A_* = 1/2$ to recover the behavior of an inert-face swimmer according to (3.15). Hydrodynamic rotation re-orients positive-mobility swimmers away from the wall at small H, unless contact is made. Swimmers with negative mobility, not pictured, are both attracted to the wall and rotated towards it, ensuring a collision.

Comparison with Numerical Results We compare this analysis with that of Uspal et al. [4], who investigate the Janus particle near a wall by numerically solving for the concentration and resulting motion of the particle. Their analysis reproduces the behavior seen in Fig. 6, but they also observe behavior which this section's analysis is unable to explain, since they consider particles with more general surface patterning. While they, like Ibrahim and Liverpool [13], study a two-hemispheres configuration with one inert face, they allow the relative size and mobilities of the two faces to differ.

In their results, a steady "sliding state," where the swimmer translates parallel to a wall at constant orientation, was observed for two classes of positive-mobility particle: those with small inert-to-active cap size ratios and small inert-to-active mobility ratios. Since the equations of motion derived here have non-zero $d\Theta/d\tau$ for all $|\Theta| < \pi/2$, no such sliding state is possible in this analysis. This is unsurprising, since we assumed constant mobility and equal cap size.

4 Case Studies, Two Dimensions

In this section, we will consider the two-dimensional analogues for a Janus swimmer in unbounded fluid and near a wall, as outlined by Crowdy [10]. We will see that exact solutions can be found for a Janus particle of variable cap size in both environments, through the use of complex variables and conformal mapping. The confined case will provide indirect evidence for the existence of the sliding state observed by Uspal et al. [4].

4.1 Unbounded Fluid

In this section, we follow Crowdy [10] to find the swimming speed of a circular Janus particle in unbounded fluid. The relevant conclusions from previous sections are

$$\boldsymbol{U} = -\frac{1}{2\pi}\int_0^{2\pi} \boldsymbol{u}_s \, d\varphi, \tag{2.14}$$

$$\boldsymbol{u}_s = M\left(\underline{\underline{I}} - \hat{\boldsymbol{n}}\hat{\boldsymbol{n}}\right)\cdot\boldsymbol{\nabla} c, \tag{2.24}$$

$$\nabla^2 c = 0, \quad \hat{\boldsymbol{n}}\cdot\boldsymbol{\nabla} c = -\frac{A}{D}, \tag{2.28}$$

Surface Geometry We parametrize the two-dimensional plane using the complex variable $z = x + iy$. Since the previous section established that swimming speed is independent of particle size for the fixed-flux boundary condition, we define our swimmer as a circular particle of unit radius. The surface is given by $e^{i\varphi}$, where φ is the angle from the symmetry axis $\hat{\boldsymbol{u}} = \hat{\boldsymbol{x}}$. We divide this boundary into two curves, C^+ and C^-, such that

$$C^+ := e^{i\varphi}, \ -\theta < \varphi < \theta, \tag{4.1}$$

and C^- consists of the remainder of the particle surface, as shown in Fig. 7. We choose piecewise constant surface activity A and mobility M such that

$$A = \begin{cases} A^+ & \text{on } C^+, \\ A^- & \text{on } C^-, \end{cases} \qquad M = \begin{cases} M^+ & \text{on } C^+, \\ M^- & \text{on } C^-, \end{cases} \tag{4.2}$$

and we denote $\beta = e^{i\theta}$, $\beta^* = e^{-i\theta}$ to be the points at which C^+ and C^- meet.

Below, we employ a conformal mapping to find the swimming speed, applying residue calculus to resolve singularities which arise due to the discontinuities at β and β^*.

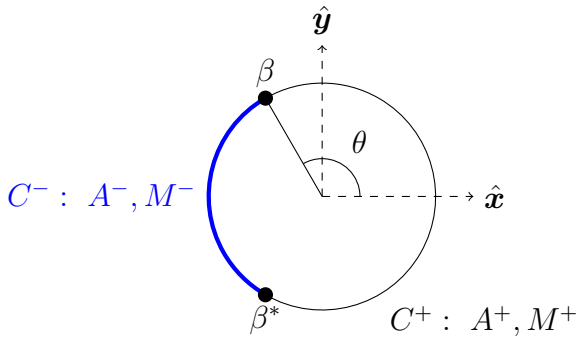

Figure 7: The two-dimensional Janus swimmer considered by Crowdy.

Concentration Distribution

Boundary Conditions We introduce $a^{\pm} = -A^{\pm}/D$ to rewrite (2.28) as

$$\hat{\boldsymbol{n}} \cdot \boldsymbol{\nabla} c = \begin{cases} a^+ & \text{on } C^+, \\ a^- & \text{on } C^-. \end{cases} \tag{4.3}$$

Crowdy chooses to specify that the particle is not a net source of solute, so that

$$2\theta a^+ + 2\left(\pi - \theta\right) a^- = 0 \implies \frac{a^- - a^+}{\pi} = \frac{a^+}{\theta - \pi}. \tag{4.4}$$

Complex Formulation Since the concentration distribution at low Péclet number is harmonic, we write it in terms of the complex analytic function $w(z)$,

$$c(x, y) = \operatorname{Re}\left\{w(z)\right\}. \tag{4.5}$$

Let $w = c(x, y) + ic'(x, y)$, $x = \left(z + z^*\right)/2$ and $y = -i\left(z - z^*\right)/2$. Then applying the chain rule to dw/dz returns the expression

$$\frac{dw}{dz} = \frac{1}{2}\left(\frac{\partial c}{\partial x} + \frac{\partial c'}{\partial y}\right) + \frac{i}{2}\left(\frac{\partial c'}{\partial x} - \frac{\partial c}{\partial y}\right), \tag{4.6}$$

but c and c' satisfy the Cauchy-Riemann relations, so

$$\frac{dw}{dz} = \frac{\partial c}{\partial x} - i\frac{\partial c}{\partial y}. \tag{4.7}$$

This implies that for some complex number $z_u = v + iw$ representing a vector $\boldsymbol{u} = v\hat{\boldsymbol{x}} + w\hat{\boldsymbol{y}}$,

$$\operatorname{Re}\left\{z_u \frac{dw}{dz}\right\} = \boldsymbol{u} \cdot \boldsymbol{\nabla} c. \tag{4.8}$$

In this way, we can rewrite the boundary conditions in terms of complex variables. If the particle surface is parametrized in a counter-clockwise fashion by its arc length s, then the complex unit tangent is $\hat{\boldsymbol{t}} = dz/ds$. The complex unit normal is this quantity rotated $\pi/2$ radians clockwise, $\hat{\boldsymbol{n}} = -i(dz/ds)$. On the unit circle, $\hat{\boldsymbol{n}} = z$ and

$$\operatorname{Re}\left\{z\frac{dw}{dz}\right\} = \begin{cases} a^+ & \text{on } C^+, \\ a^- & \text{on } C^-. \end{cases} \tag{4.9}$$

Solution for the Normal Gradient Since we assume there exists no solute in the far-field, and the particle is not a net source, the function $w(z) \sim \mathcal{O}(1/z)$, implying $z(dw/dz)$ is analytic and single-valued for $|z| > 1$. In that case, (4.9) is solved by

$$z\frac{dw}{dz} = a^+ - \frac{i(a^- - a^+)}{\pi}\log\eta(z), \tag{4.10}$$

where the function $\eta(z)$ is the Mobius map

$$\eta(z) = \mathcal{A}\left(\frac{z-\beta}{z-\beta^*}\right), \quad \mathcal{A} = e^{i(\pi-\theta)}, \tag{4.11}$$

which unfolds the swimmer body onto the real numbers in the η-plane such that C^+ and C^- are mapped to the positive and negative real lines, respectively. The points β and β^* map to the origin and infinity, and we have chosen the branch of the logarithm so that

$$\mathrm{Im}\left\{\log\eta(z)\right\} = \begin{cases} 0 & \text{on } C^+ \\ \pi & \text{on } C^-. \end{cases} \tag{4.12}$$

Swimming Speed On the unit circle, the tangent $\hat{\boldsymbol{t}} = iz$, so the tangential gradient is

$$\left(\underline{\underline{I}} - \hat{\boldsymbol{n}}\hat{\boldsymbol{n}}\right)\cdot\boldsymbol{\nabla}c = \hat{\boldsymbol{t}}\hat{\boldsymbol{t}}\cdot\boldsymbol{\nabla}c = iz\mathrm{Re}\left\{iz\frac{dw}{dz}\right\}. \tag{4.13}$$

Substituting (4.10) and (4.13) into (2.24) yields the slip velocity

$$u_s = \begin{cases} \dfrac{izM^+(a^- - a^+)}{\pi}\log|\eta(z)| & \text{on } C^+, \\ \dfrac{izM^-(a^- - a^+)}{\pi}\log|\eta(z)| & \text{on } C^-, \end{cases} \tag{4.14}$$

which we substitute into (2.14), obtaining the swimming speed

$$U = -\frac{M^+(a^- - a^+)}{2\pi^2}\int_{C^+}\log|\eta(z)|dz - \frac{M^-(a^- - a^+)}{2\pi^2}\int_{C^-}\log|\eta(z)|dz. \tag{4.15}$$

These integrals can be evaluated using residue calculus to find an analytic solution to U.

Residue Calculation Inverting and differentiating (4.11) yields

$$\frac{dz}{d\eta} = \frac{\mathcal{A}\left(\beta - \beta^*\right)}{\left(\eta - \mathcal{A}\right)^2} =: P(\eta), \tag{4.16}$$

a relation we use to rewrite the integrals within (4.15) in terms of η, finding

$$U = -\frac{M^+(a^- - a^+)}{2\pi^2}\int_{\infty}^{0}\log|\eta|P(\eta)d\eta - \frac{M^-(a^- - a^+)}{2\pi^2}\int_{0}^{-\infty}\log|\eta|P(\eta)d\eta. \tag{4.17}$$

Because these integrals contain a pole at $\eta = \mathcal{A}$, we calculate the residues

$$\begin{aligned} \mathrm{Res}\left[P(\eta)\right] &= \lim_{\eta\to\mathcal{A}}\frac{d}{d\eta}\left[\mathcal{A}(\beta-\beta^*)\right] = 0, \\ \mathrm{Res}\left[P(\eta)\log\eta\right] &= \lim_{\eta\to\mathcal{A}}\frac{d}{d\eta}\left[\mathcal{A}(\beta-\beta^*)\log\eta\right] = \beta - \beta^* = 2i\sin\theta, \\ \mathrm{Res}\left[P(\eta)\left(\log\eta\right)^2\right] &= \lim_{\eta\to\mathcal{A}}\frac{d}{d\eta}\left[\mathcal{A}(\beta-\beta^*)\left(\log\eta\right)^2\right] = 2(\beta-\beta^*)\log = -4(\pi-\theta)\sin\theta, \end{aligned} \tag{4.18}$$

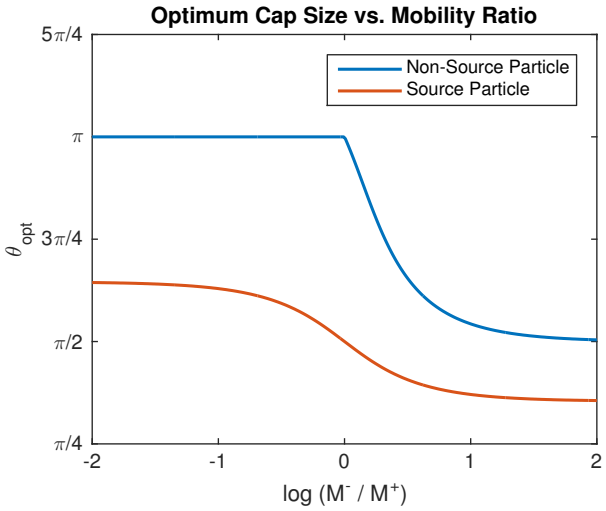

Figure 8: The optimum cap size θ_{opt} corresponding to maximum velocity for a given ratio of mobilities M^-/M^+ is numerically computed for 1) Crowdy's non-source swimmer and 2) an identical swimmer which can act as a source of solute.

and substitute them into the following relations, simplified from their presentation in Appendix B of Crowdy [10],

$$\begin{aligned}\int_{\infty}^{0} \log|\eta| P(\eta) d\eta &= -i\pi \text{Res}\left[P(\eta)\log\eta\right] + \frac{1}{2}\text{Res}\left[P(\eta)(\log\eta)^2\right] = 2\theta\sin\theta, \\ \int_{0}^{-\infty} \log|\eta| P(\eta) d\eta &= -\frac{1}{2}\text{Res}\left[P(\eta)(\log\eta)^2\right] = 2(\pi-\theta)\sin\theta.\end{aligned} \tag{4.19}$$

Combining these relations with (4.17) yields

$$U = -\frac{(a^- - a^+)\sin\theta\left[M^+\theta + M^-(\pi-\theta)\right]}{\pi^2}. \tag{4.20}$$

Finally, to satisfy the requirement that the particle is not a net source of solute, we apply the relation (4.4) and find the unbounded swimming speed

$$\boxed{U = -\frac{A^+\sin\theta\left[M^+\theta + M^-(\pi-\theta)\right]}{D\pi(\pi-\theta)}.} \tag{4.21}$$

Discussion With this result, we can examine the effects of different cap sizes and mobilities in three dimensions, since the two-dimensional case is likely to behave in a qualitatively similar way. Consider the question of what optimum cap size yields the maximum velocity for a given activity A^+ and mobility ratio $\lambda = M^-/M^+$. Numerically solving (4.21), as I have in Fig. 8, reveals that the optimum configuration for $\lambda \leq 1$ is a uniform surface activity a^+ punctuated by a single site of absorption at one end. For $\lambda > 1$, an optimum cap size θ_{opt} exists, which approaches $\pi/2$ as λ approaches infinity.

Since the work of Golestanian et al. [6] established that the unbounded swimming speed of a Janus particle is unrelated to its net source strength, I temporarily suspended the no net source prescription and numerically solved (4.20) for a range of λ as well. For a particle with a given activity difference $A^+ - A^-$, an optimum cap size θ_{opt} exists for all possible λ. Showing this analytically in three dimensions would have been much more difficult using the formalism of previous sections. In the next section, similar analysis will suggest indirect evidence for a sliding state.

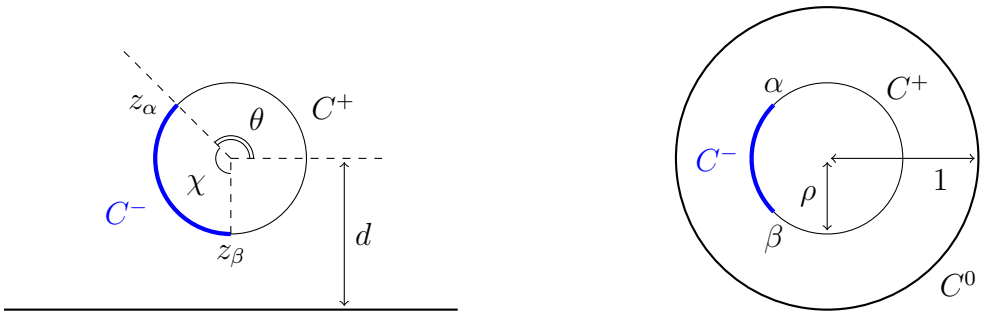

(a) (b)

Figure 9: The mapping defined in (4.22) maps the annulus pictured above in (b) to the doubly connected fluid above the wall in (a). The points α and β map to z_α and z_β. In general, α and β are not symmetric about the x axis in the preimage ζ-plane.

4.2 Near Infinite Wall

Continuing Crowdy's analysis, we examine a particle near a wall. By employing the same methods as in the unbounded case, we find an exact solution which will allow for the qualitative examination of swimmer behavior in the case of unequal cap sizes.

Wall Geometry and Conformal Mapping Let the wall lie directly on the x-axis, and consider a nearby, circular particle of radius s, located at the point $(0, d)$. The problem will be treated within a preimage annulus, parametrized by $|\zeta| \in [\rho, 1]$. As shown in Fig. 9, the two regions are related by the Mobius map

$$z(\zeta) = iR\left(\frac{\zeta+1}{\zeta-1}\right), \tag{4.22}$$

where ρ and R are given by

$$\rho = \frac{d}{s} - \sqrt{\left(\frac{d}{s}\right)^2 - 1}, \quad R = d\left(\frac{\rho^2-1}{\rho^2+1}\right). \tag{4.23}$$

The discontinuous points on the particle boundary, now denoted z_α and z_β, satisfy

$$z_\alpha = id + se^{i\theta}, \quad z_\beta = id + s^{i(\theta+\chi)}, \tag{4.24}$$

where the parameter θ has been redefined to measure the instantaneous tilt angle of the point z_α relative to the $\hat{\boldsymbol{x}}$ axis and χ is the cap size of C^-. The swimmer velocities are

$$\boldsymbol{U} = (U, V, 0), \quad \boldsymbol{\Omega} = (0, 0, \Omega). \tag{4.25}$$

Reciprocal Theorem Each time we have used the reciprocal theorem thus far, we have done so with regard to an unbounded flow. Now, however, it must be applied with regard to the geometry at hand, and the dragging flow considered must be a that of an infinite cylinder being towed or rotated near an infinite wall.

In a previous paper [17], Crowdy establishes that the relevant dragging problem can be solved within the preimage ζ-plane introduced by (4.22), such that the right side of the general reciprocal theorem (2.10) can be written in two dimensions as

$$-\oint_{|z-z_d|=s} \boldsymbol{u}_s \cdot \underline{\underline{\sigma_2}} \cdot \hat{\boldsymbol{n}}\, ds = -\mathrm{Re}\left\{2\mu i \oint_{|\zeta|=\rho} \boldsymbol{u}_s^* \frac{d\mathcal{H}}{d\zeta} d\zeta\right\}, \tag{4.26}$$

where μ is the dynamic viscosity and $d\mathcal{H}/d\zeta$ is an analytic function depending on which dragging problem is considered. We will take these functions as given in later sections.

Concentration Distribution

Boundary Conditions We denote the wall as the boundary C^0 and specify that it allows no solute flux, so that the complete set of boundary conditions is

$$\hat{\boldsymbol{n}} \cdot \boldsymbol{\nabla} c = \begin{cases} 0 & \text{on } C^0, \\ a^+ & \text{on } C^+, \\ a^- & \text{on } C^-. \end{cases} \tag{4.27}$$

Again, we specify that the particle is not a net source of solute, so that

$$a^-\chi + a^+(2\pi - \chi) = 0 \implies (a^- - a^+) = -\frac{2\pi a^+}{\chi}. \tag{4.28}$$

and the far-field concentration is $\mathcal{O}(1/z)$.

Complex Formulation As in the unbounded case, we write $c = \mathrm{Re}\{w(z)\}$. Recall that the complex unit tangent and normal are given by dz/ds and $-i(dz/ds)$. We use this fact to rewrite (4.27) in the complex form

$$\mathrm{Re}\left\{-i\frac{dz}{ds}\frac{dw}{dz}\right\} = \begin{cases} 0 & \text{on } C^0, \\ a^+ & \text{on } C^+, \\ a^- & \text{on } C^-. \end{cases} \tag{4.29}$$

We write the unit tangent in terms of ζ by applying the chain rule to find

$$\hat{\boldsymbol{t}} = \frac{dz}{ds} = \frac{dz}{d\zeta}\frac{d\zeta}{ds_\zeta}\frac{ds_\zeta}{ds}, \tag{4.30}$$

where the arc length s parameterizes the boundary $z(s)$. In the ζ-plane, the arc length s_ζ parameterizes $\zeta(s_\zeta)$. Finally, ds_ζ/ds, the ratio between the two planes' arc lengths, is $|dz/d\zeta|^{-1}$. The counter-clockwise and clockwise unit tangents on $|\zeta| = 1$ and ρ are

$$\frac{dz}{ds} = -\frac{i\zeta z'(\zeta)}{|z'(\zeta)|} \text{ on } C^0, \quad \frac{dz}{ds} = \frac{i\zeta z'(\zeta)}{\rho|z'(\zeta)|} \text{ on } C^+, C^-, \tag{4.31}$$

and we rewrite the boundary conditions (4.29) as

$$\mathrm{Re}\left\{\frac{dw}{dz}\zeta z'(\zeta)\right\} = \begin{cases} 0 & \text{on } C^0, \\ \rho a^+|z'(\zeta)| & \text{on } C^+, \\ \rho a^-|z'(\zeta)| & \text{on } C^-. \end{cases} \tag{4.32}$$

We find the explicit representation for $|z'(\zeta)|$ on $|\zeta| = \rho$ by differentiating (4.22) and multiplying by the complex conjugate to obtain

$$z'(\zeta) = -\frac{2iR}{(\zeta-1)^2}, \qquad |z'(\zeta)|\Big|_{|\zeta|=\rho} = \boxed{-\frac{2R\zeta}{(\zeta-1)\left(\rho^2-\zeta\right)} := X(\zeta).} \tag{4.33}$$

As expected, $X(\zeta)$ is a real, positive function on $|\zeta| = \rho$.

Managing Singularities The function on the left side of (4.32) must be analytic at $\zeta = 1$, corresponding to $z \to \infty$, because of the far-field condition $w(z) \sim \mathcal{O}(1/z)$. At the same time, we expect logarithmic singularities at $\zeta = \alpha, \beta$ due to the discontinuous boundary conditions. To account for these, we define the function

$$\boxed{G(\zeta) = -X(\zeta)\left[\rho a^+ - \frac{i\rho(a^- - a^+)}{\pi}\log\eta(\zeta)\right],} \tag{4.34}$$

where we have re-introduced a variant of the η-mapping,

$$\eta(\zeta) = \mathcal{A}\left(\frac{\zeta-\alpha}{\zeta-\beta}\right), \quad \mathcal{A} = e^{i\gamma}, \quad \gamma = \frac{1}{2}\arg\left(\frac{\beta}{\alpha}\right), \tag{4.35}$$

which takes $|\zeta| = \rho$ to the real numbers in the η-plane. We choose the branch of the logarithm so that C^+ and C^- are again mapped to the positive and negative real lines.

While Crowdy writes $\mathcal{A} = e^{i(\pi-\gamma)}$ [10], this is a typographical error. Consider as an illustration the case where α is in the second quadrant so that its real part is negative, $\beta = \alpha^*$ so that $\pi = \arg(\alpha) + \gamma$, and $\zeta = -\alpha$. In that case,

$$\arg\left(\frac{\zeta-\alpha}{\zeta-\beta}\right) = \arg\left(\frac{\alpha}{\mathrm{Re}\{\alpha\}}\right) = \arg(\alpha) - \pi = -\gamma. \tag{4.36}$$

For $\eta(-\alpha)$ to lie on the positive real-η line as desired, we must have $\mathcal{A} = e^{i\gamma}$.

The real part of $-G(\zeta)$ satisfies the boundary conditions on C^+ and C^- in (4.32), so adding $G(\zeta)$ to both sides produces the boundary problem

$$\mathrm{Re}\left\{\frac{dw}{dz}\zeta z'(\zeta) + G(\zeta)\right\} = \begin{cases} \mathrm{Re}\{G(\zeta)\} & \text{on } C^0, \\ 0 & \text{on } C^+, \\ 0 & \text{on } C^-, \end{cases} \tag{4.37}$$

where we have transferred the logarithmic singularities on $|\zeta| = \rho$ to our solution function so they can be explicitly resolved using residue calculus.

Since $G(\zeta)$ has a pole at $\zeta = 1$ within $X(\zeta)$, we define

$$\boxed{J(\zeta) = X(\zeta)\left[\rho a^+ - \frac{i\rho(a^- - a^+)}{\pi}\log\eta(1)\right],} \tag{4.38}$$

and add it to both sides so that

$$\mathrm{Re}\left\{\frac{dw}{dz}\zeta z'(\zeta) + G(\zeta) + J(\zeta)\right\} = \begin{cases} \mathrm{Re}\{G(\zeta) + J(\zeta)\} & \text{on } C^0, \\ \mathrm{Re}\{J(\zeta)\} & \text{on } C^+, \\ \mathrm{Re}\{J(\zeta)\} & \text{on } C^-. \end{cases} \tag{4.39}$$

Note that as ζ approaches 1, the sum $G(\zeta) + J(\zeta)$ satisfies the proportion

$$G(\zeta) + J(\zeta) \propto \frac{1}{\xi - 1} \log\left(\frac{\eta(\zeta)}{\eta(1)}\right), \tag{4.40}$$

so the boundary condition on C_0 now remains smooth at $\zeta \to 1$.

Finally, applying the no net source prescription (4.28), $J(\zeta)$ simplifies to

$$J(\zeta) = X(\zeta)\rho a^+ \left[1 + \frac{2i}{\chi} \log \eta(1)\right]. \tag{4.41}$$

It can be shown that $\mathrm{Im}\{\log \eta(1)\} = \chi/2$. Since $X(\zeta)$ was defined to be real on $|\zeta| = \rho$, $\mathrm{Re}\{J(\zeta)\}$ must vanish on the particle boundary, and the boundary conditions reduce to

$$\mathrm{Re}\{I(\zeta)\} = \begin{cases} \mathrm{Re}\{G(\zeta) + J(\zeta)\} & \text{on } |\zeta| = 1, \\ 0 & \text{on } |\zeta| = \rho. \end{cases} \tag{4.42}$$

where we have defined

$$\boxed{I(\zeta) := \frac{dw}{dz}\zeta z'(\zeta) + G(\zeta) + J(\zeta).} \tag{4.43}$$

Solution As desired, all singularities are confined to the left side of the equation, where they can be analytically treated. The problem (4.42) can be readily solved as a modified Schwarz problem, treated in an earlier paper by Crowdy [18]. The solution is

$$I(\zeta) = c_0 + \sum_{n=1}^{\infty} c_n \zeta^n + \sum_{n=1}^{\infty} \frac{c_{-n}\rho^n}{\zeta^n}, \quad \rho < |\zeta| < 1, \tag{4.44}$$

for some set of coefficients $\{c_n\}$. The boundary condition on C^0 is known to be smooth and analytic, so we decompose it into a set of Fourier coefficients $\{d_n\}$, satisfying

$$\mathrm{Re}\{G(\zeta) + J(\zeta)\}\Big|_{|\zeta|=1} = \sum_{n=-\infty}^{\infty} d_n \zeta^n. \tag{4.45}$$

Combining (4.44) and (4.45) fixes the coefficients $\{c_n\}$, yielding

$$\mathrm{Re}\{c_0\} = d_0, \quad c_n = \frac{2d_n}{1 - \rho^{2n}}, \quad c_{-n} = -\frac{2\rho^n d_n^*}{1 - \rho^{2n}}, \quad n \geq 1, \tag{4.46}$$

so that $I(\zeta)$ is a known function. At this point, we can compute the slip velocity over the particle surface, using

$$\boxed{\frac{dw}{dz}\zeta z'(\zeta) = I(\zeta) - G(\zeta) - J(\zeta).} \tag{4.47}$$

Slip Velocity The slip velocity (2.24) is written in complex form as

$$\boldsymbol{u}_s = M\mathrm{Re}\left\{\frac{dz}{ds}\frac{dw}{dz}\right\}\frac{dz}{ds}. \tag{4.48}$$

To find this value, we substitute in the expressions for the complex tangent on $|\zeta| = \rho$ (4.31), the derivative $z'(\zeta)$ and its magnitude $|z'(\zeta)| = X(\zeta)$ (4.33), and, finally, the function we have just found (4.47). After taking the complex conjugate, this yields

$$\boldsymbol{u}_s^* = M \text{ Re}\left\{\frac{i(\zeta-1)(\zeta-\rho^2)}{2R\zeta}\left[I(\zeta)-G(\zeta)-J(\zeta)\right]\right\}\frac{1-\zeta}{\rho^2-\zeta}, \tag{4.49}$$

which we separate into regular and singular parts

$$\boldsymbol{u}_s^{*(r)} = M \text{ Re}\left\{\frac{i(\zeta-1)(\zeta-\rho^2)}{2R\zeta}I(\zeta)\right\}\frac{1-\zeta}{\rho^2-\zeta}, \tag{4.50}$$

$$\boldsymbol{u}_s^{*(s)} = M \text{ Re}\left\{\frac{i(\zeta-1)(\zeta-\rho^2)}{2R\zeta}\left[-G(\zeta)-J(\zeta)\right]\right\}\frac{1-\zeta}{\rho^2-\zeta}, \tag{4.51}$$

because of the logarithmic singularities in $\text{Re}\{G(\zeta)+J(\zeta)\}$ on $|\zeta|=\rho$. These are revealed by simplifying the latter integral to obtain

$$\boldsymbol{u}_s^{*(s)} = M \text{ Re}\left\{\frac{\rho(a^- - a^+)}{\pi}\log\left(\frac{\eta(\zeta)}{\eta(1)}\right)\right\}\frac{1-\zeta}{\rho^2-\zeta}, \tag{4.52}$$

and noting $\eta(\alpha)=0$ and $\eta(\beta)\to\infty$.

At this point, Crowdy stipulates a constant mobility $M=1$ everywhere on the particle. While this prescription eliminates the mobility-ratio sliding state observed by Uspal et al. [4], the smaller solution space greatly simplifies the remaining analysis.

The slip velocity is now a known function on the particle surface. In the next section, we calculate the particle velocities $\boldsymbol{U}$ and $\boldsymbol{\Omega}$.

Swimming Speeds As before, we relate the diffusiophoretic slip velocity to the particle motion through the reciprocal theorem, which is given by (2.10) and (4.26) to be

$$\boxed{\boldsymbol{U}\cdot\boldsymbol{F}' + \boldsymbol{\Omega}\cdot\boldsymbol{T}' = -\text{Re}\left\{2\mu i\oint_{|\zeta|=\rho}\left[\boldsymbol{u}_s^{*(s)}+\boldsymbol{u}_s^{*(r)}\right]\frac{d\mathcal{H}}{d\zeta}d\zeta\right\}.} \tag{4.53}$$

We will apply this to three different dragging flows: a cylinder moving parallel to a wall, a cylinder moving perpendicular to a wall, and a cylinder rotating near a wall. The function $d\mathcal{H}/d\zeta$ takes on different smooth, analytic forms for each of these situations, known from Crowdy's past work [17]. The integral on the right side of (4.53) is computed as follows.

Regular Portion The regular slip function $\boldsymbol{u}_s^{*(r)}$ on $|\zeta|=\rho$ can be written as the Laurent expansion

$$\boldsymbol{u}_s^{*(r)} = \sum_{n=0}^{\infty} b_n\zeta^n + b_n^*\frac{\rho^{2n}}{\zeta^n}, \tag{4.54}$$

where the $\{b_n\}$ are known coefficients given the $\{c_n\}$ fixed in (4.46). Since $\boldsymbol{u}_s^{*(r)}$ and $d\mathcal{H}/d\zeta$ are both smooth and analytic on $|\zeta|=\rho$, the integral can be computed by means of the residue theorem. Doing so reveals that only b_0 and b_1 contribute to the velocities.

Singular Portion The singular integral can be evaluated exactly as in the unbounded case, by rewriting the integrand as a function of η and integrating over the real η-line. The resulting integrals take the form

$$I_1 = \int_{\infty}^{0} f(\eta) \log|\eta| d\eta, \quad I_2 = \int_{0}^{-\infty} f(\eta) \log|\eta| d\eta, \tag{4.55}$$

and can be evaluated using residue calculus as in the unbounded case. Since $f(\eta)$ can have multiple poles, the relations analogous to (4.19) become more complicated.

Dragging Flows Now, to calculate the velocities $\boldsymbol{U} = (U, V, 0)$ and $\boldsymbol{\Omega} = (0, 0, \Omega)$, we apply the reciprocal theorem (4.53) to the three dragging flows.

Parallel Motion First, we determine the parallel speed U by considering the cylinder being dragged along an infinite wall at unit velocity. From Crowdy [17],

$$\frac{d\mathcal{H}}{d\zeta} = \frac{2F_d}{(1-\rho^2)}\left(1 + \frac{(1-\rho^2)}{\zeta} - \frac{\rho^2}{\zeta^2}\right), \quad F_d = -\frac{1}{\log\rho^2}. \tag{4.56}$$

which corresponds to a dragging force

$$\boldsymbol{F'} = (-8\pi\mu F_d, 0, 0)\,. \tag{4.57}$$

Evaluating the $\boldsymbol{u}_s^{*(r)}$ integral yields the regular velocity contribution

$$\begin{aligned} U^{(r)} &= \mathrm{Re}\left\{\frac{i}{4\pi F_d}\oint_{|\zeta|=\rho} \boldsymbol{u}_s^{*(r)} \frac{d\mathcal{H}}{d\zeta} d\zeta\right\} \\ &= \rho \mathrm{Re}\left\{b_1\right\} \\ &= \frac{2a^+\rho}{\chi(1-\rho^2)} \log\left|\frac{1-\beta}{1-\alpha}\right| - \frac{2\rho^3 a^+}{\chi(1-\rho^4)} \mathrm{Re}\left\{\beta - \alpha\right\}, \end{aligned} \tag{4.58}$$

and evaluating the $\boldsymbol{u}_s^{*(s)}$ integral using residue calculus yields the singular contribution

$$\begin{aligned} U^{(s)} &= \mathrm{Re}\left\{\frac{i}{4\pi F_d}\oint_{|\zeta|=\rho} \boldsymbol{u}_s^{*(s)} \frac{d\mathcal{H}}{d\zeta} d\zeta\right\} \\ &= \frac{a^+}{\chi}\frac{\rho}{1-\rho^2}\left[(\beta-\alpha)\left(1 + \frac{1}{\alpha\beta}\right)\right], \end{aligned} \tag{4.59}$$

so that the value of U is the sum $U^{(r)} + U^{(s)}$.

Perpendicular Motion Now, we determine the perpendicular speed V by considering a cylinder moving directly away from a wall at unit speed. From Crowdy [17],

$$\frac{d\mathcal{H}}{d\zeta} = 2F_d\left(\frac{1}{\zeta} - \frac{\rho^2}{(1+\rho^2)\zeta^2} - \frac{1}{1+\rho^2}\right), \quad F_d = -\frac{i}{2(1-\rho^2)/(1+\rho^2) + \log\rho^2}, \tag{4.60}$$

and the particle drag is

$$\boldsymbol{F'} = (0, 8\pi\mu i F_d, 0)\,. \tag{4.61}$$

The smooth contribution is found to be

$$\begin{aligned} V^{(r)} &= -\mathrm{Re}\left\{\frac{1}{4\pi F_d}\oint_{|\zeta|=\rho} \boldsymbol{u}_s^{*(r)}\frac{d\mathcal{H}}{d\zeta}d\zeta\right\} \\ &= -\frac{\rho(1-\rho^2)}{(1+\rho^2)}\mathrm{Im}\left\{b_1\right\} \\ &= -\frac{2a^+}{\chi}\frac{\rho(1-\rho^2)}{(1+\rho^2)}\left[\frac{\rho^2}{(1-\rho^4)}\mathrm{Im}\left\{\beta-\alpha\right\}+\frac{1}{(1-\rho^2)}\mathrm{arg}\left[\frac{1-\beta^*}{1-\alpha^*}\right]\right], \end{aligned} \tag{4.62}$$

and the singular contribution is

$$\begin{aligned} V^{(s)} &= -\mathrm{Re}\left\{\frac{1}{4\pi F_d}\oint_{|\zeta|=\rho} \boldsymbol{u}_s^{*(s)}\frac{d\mathcal{H}}{d\zeta}d\zeta\right\} \\ &= \frac{a^+}{\chi}\frac{\rho}{1+\rho^2}\mathrm{Im}\left\{(\alpha\beta-1)\left(\frac{1}{\alpha}-\frac{1}{\beta}\right)\right\}. \end{aligned} \tag{4.63}$$

As before, $V = V^{(r)} + V^{(s)}$.

Rotation Finally, to compute the angular velocity Ω, we consider the stationary cylinder rotated near a wall at unit angular velocity. From Crowdy [17],

$$\frac{d\mathcal{H}}{d\zeta} = \frac{4R\rho^2}{(1-\rho^2)^3}\left(1-\frac{\rho^2}{\zeta^2}\right)+\frac{2R}{(\zeta-1)^2}, \tag{4.64}$$

and its corresponding torque is

$$\boldsymbol{T'} = \left(0, 0, -4\pi s^2\frac{(1+\rho^2)}{(1-\rho^2)}\right). \tag{4.65}$$

The regular portion is

$$\begin{aligned} \Omega^{(r)} &= -\mathrm{Re}\left\{\frac{2\mu i}{T'_z}\oint_{|\zeta|=\rho} \boldsymbol{u}_s^{*(r)}\frac{d\mathcal{H}}{d\zeta}d\zeta\right\} \\ &= -\frac{b_0}{s}-\frac{4\pi\rho^2}{(2\pi-\chi)(1+\rho^2)}\mathrm{Re}\left\{b_1\right\} \\ &= \frac{4a}{s\chi}\frac{\rho^4}{(1-\rho^4)}\left[\log\left|\frac{1-\beta}{1-\alpha}\right|+\frac{1}{(1+\rho^2)}\mathrm{Re}\left\{\beta-\alpha\right\}\right] \end{aligned} \tag{4.66}$$

and the singular portion is

$$\begin{aligned} \Omega^{(s)} &= -\mathrm{Re}\left\{\frac{2\mu i}{T'_z}\oint_{|\zeta|=\rho} \boldsymbol{u}_s^{*(s)}\frac{d\mathcal{H}}{d\zeta}d\zeta\right\} \\ &= -\frac{2a}{s\chi}\left[\log\left|\frac{1-\alpha}{1-\beta}\right|+\frac{\rho^2}{1-\rho^4}\mathrm{Re}\left\{(\beta-\alpha)\left(1+\frac{1}{\alpha\beta}\right)\right\}\right]. \end{aligned} \tag{4.67}$$

The total angular velocity is $\Omega = \Omega^{(r)} + \Omega^{(s)}$.

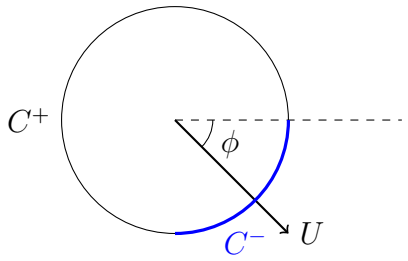

Figure 10: For $a < 0$, the particle moves in the direction of C^-. The orientation is parametrized by ϕ, the tilt angle between the midpoint of C^- and the x axis.

Equations of Motion At this point, we determine the time evolution of a two-dimensional Janus particle near an infinite wall. If the particle is located at the position (X, Y), and θ is defined as in Fig. 9, then we identify

$$\dot{X} = U, \;\; \dot{Y} = V, \;\; \dot{\theta} = \Omega, \tag{4.68}$$

where these are the values that have just been determined above. The following are the equations of motion for the system, as determined by Crowdy [10].

$$\begin{aligned}
\frac{dX}{dt} &= \frac{a^+\rho}{\chi(1-\rho^2)}\left[\frac{1-\rho^2}{1+\rho^2}\mathrm{Re}\left\{\beta-\alpha\right\} + \mathrm{Re}\left\{\frac{1}{\alpha}-\frac{1}{\beta}\right\} + 2\log\left|\frac{1-\beta}{1-\alpha}\right|\right], \\
\frac{dY}{dt} &= \frac{a^+\rho}{\chi(1+\rho^2)}\left[\frac{1-\rho^2}{1+\rho^2}\mathrm{Im}\left\{\beta-\alpha\right\} - \mathrm{Im}\left\{\frac{1}{\alpha}-\frac{1}{\beta}\right\} + 2\,\arg\left[\frac{1-\beta}{1-\alpha}\right]\right], \\
\frac{d\theta}{dt} &= -\frac{2a^+\rho^2}{s\chi(1-\rho^4)}\left[\frac{1-\rho^2}{1+\rho^2}\mathrm{Re}\left\{\beta-\alpha\right\} + \mathrm{Re}\left\{\frac{1}{\alpha}-\frac{1}{\beta}\right\} - \frac{1+\rho^4}{\rho^2}\log\left|\frac{1-\beta}{1-\alpha}\right|\right],
\end{aligned} \tag{4.69}$$

with the parameters ρ, α and β given by

$$\rho = \frac{Y}{s} - \sqrt{\left(\frac{Y}{s}\right)^2 - 1}, \;\; \alpha = \frac{\rho^2 - i\rho e^{i\theta}}{1 - i\rho e^{i\theta}}, \;\; \beta = \frac{\rho^2 - i\rho e^{i(\theta+\chi)}}{1 - i\rho e^{i(\theta+\chi)}}. \tag{4.70}$$

Discussion Since we consider a positive-mobility particle, we set $a < 0$ so that C^- will act as the nose of the swimmer. In that case, $\phi = \theta + \chi/2$, the tilt angle of C^-'s midpoint and the x axis as shown in Fig. 10, is a convenient measure of the swimmer's orientation. As before, due to symmetry, we need only consider $|\phi| \leq \pi/2$. These equations can be numerically integrated to observe trajectories of the particle, as in previous sections.

Equal Cap Size For equal cap sizes $\chi = \pi$, the behavior witnessed is qualitatively the same as that shown in Fig. 6. Swimmers which approach the wall either hit in finite time or re-orient away due to rotation away from the wall in all possible orientations ϕ.

Unequal Cap Size If we allow $\chi \neq \pi$, there do exist orientations with rotation towards the wall. At any distance d, there exists some critical cap size χ_{crit} such that $\chi < \chi_{\text{crit}}$ implies the existence of orientations with $d\theta/dt < 0$. This means there also

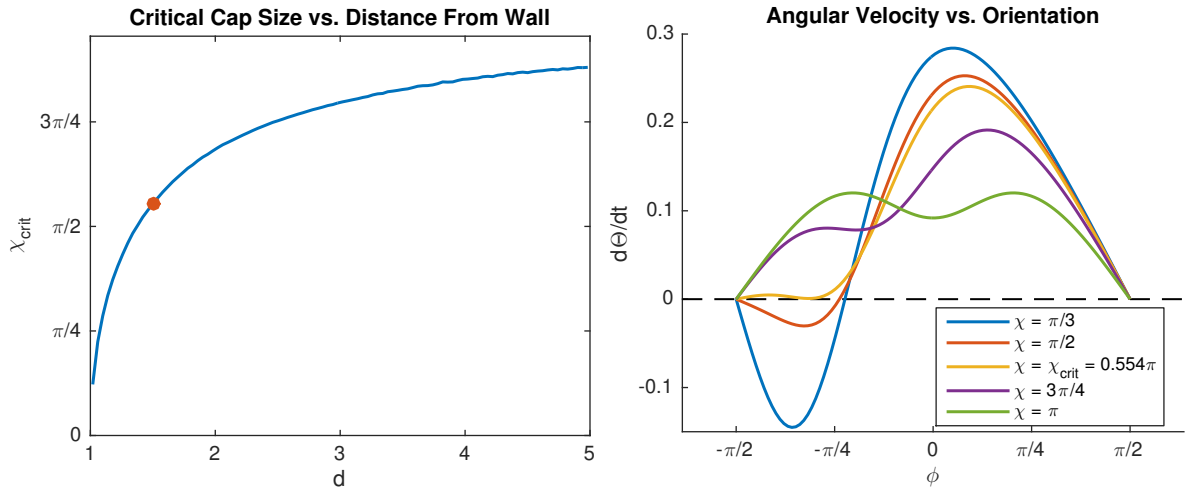

(a) (b)

Figure 11: (a) The variation of the critical cap size χ_{crit} with distance from the wall d is shown. As $d \to s$, $\chi_{\text{crit}} \to 0$, so all orientations begin rotating the particle away from the wall. (b) For $d = 1.5s$, the orange dot in (a), the orientation ϕ vs. angular velocity $d\theta/dt$ is displayed for several cap sizes χ. If $\chi \leq \chi_{\text{crit}}$, orientations exist with no rotation.

exist orientations for which there is no rotation, demonstrated in Fig. 11, where I have numerically investigated how χ_{crit} varies with d.

While the equations of motion above do not support a sliding state, this can likely be attributed to the particle not being a net source of solute. The analysis of Ibrahim and Liverpool [13] showed the only effect of the source strength A_0 is to induce repulsion from the wall. If this conclusion holds in two dimensions, and the particle in Crowdy's analysis is allowed to be a net source, a wise choice of A_0 could exactly offset dY/dt at the orientation for which $d\theta/dt = 0$, yielding the sliding state observed by Uspal et al. [4].

5 Extension to Other Geometries

At this point, I extend the previous section's results to other environments by conformally mapping them to the half plane $y > 0$, where Crowdy's solution (4.69) can be applied. While the process is not rigorous, it could provide insight into confinement effects of these geometries on Janus swimmers. Below, I list the approximations used to complete the analysis and present results for a particle near a corner and in a semi-infinite channel.

Boundary Warping Conformal mappings from many regions to the half plane are well known and easy to manipulate, but they do not generally map a circular particle boundary to a circle in the half plane. I address this shortcoming by approximating mapped swimmer boundaries with circular replacements of the same area and centroid, as shown in Fig. 12. This process introduces an asymmetry which could drive behavior unrelated to actual particle dynamics. The potential strength of this effect, linked to the warping undergone by the boundary during the mapping process, can be estimated by the eccentricity

$$e = \sqrt{1 - \frac{r_{\text{min}}^2}{r_{\text{max}}^2}}, \tag{5.1}$$

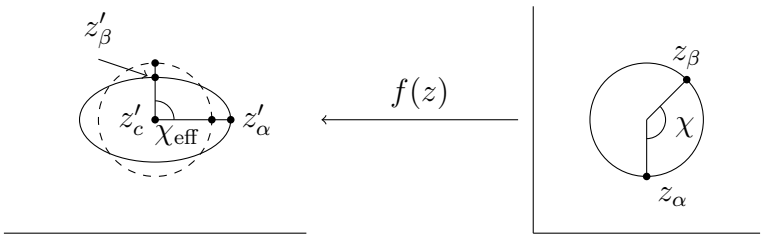

Figure 12: A mapping $f(z)$ sends the circular particle in the quarter-plane at right to the solid boundary in the half-plane at left. In the half plane, the swimmer's boundary can be approximated by the dashed circle, which shares the mapped boundary's area and centroid. The points z_α and z_β map to z'_α and z'_β; note the mapping alters the particle cap size χ. For reference, the eccentricity of the mapped boundary is $e = 0.8$.

where $r_{\max}$ and $r_{\min}$ are the largest and smallest distances on the true boundary from its centroid. While the warped boundary is not an ellipse, this quantity is zero for a circle and grows with the magnitude of warping induced.

Surface Geometry If a mapped particle's centroid is given by z'_c and its area by A, I calculate the following effective height Y_{eff} and radius s_{eff} to use in Crowdy's equations,

$$\boxed{Y_{\text{eff}} = \text{Im}\left\{z'_c\right\}, \quad s_{\text{eff}} = \sqrt{\frac{A}{\pi}}.} \tag{5.2}$$

As before, let z_α and z_β be the points at which C^+ and C^- meet. If these map to z'_α and z'_β, I define the effective orientation parameter θ_{eff} and cap size χ_{eff} to be

$$\boxed{\theta_{\text{eff}} = \arg\left(z'_\alpha - z'_c\right), \quad \chi_{\text{eff}} = \arg\left(z'_\beta - z'_c\right) - \arg\left(z'_\alpha - z'_c\right).} \tag{5.3}$$

Boundary Condition At this point, I attempt to define an effective surface activity a^+_{eff} on the mapped cap $(C^+)'$. Consider the fixed flux boundary condition: intuitively, as the relative size of the cap changes due to warping, the solute flux should remain proportional to the cap size times the activity, implying $a^+_{\text{eff}}(2\pi - \chi_{\text{eff}}) \propto a^+(2\pi - \chi)$.

Another consideration is to require that results of this analysis not change with an arbitrary scaling of the mapping. This is assured by requiring $a^+_{\text{eff}}(s/s_{\text{eff}}) = a^+$, so that the mapped problem is equivalent to a particle of radius s and activity a^+, within a scaling of the geometry and solute concentration. The effective surface activity which satisfies these relations is

$$\boxed{a^+_{\text{eff}} = a^+\left(\frac{s_{\text{eff}}}{s}\right)\left(\frac{2\pi - \chi}{2\pi - \chi_{\text{eff}}}\right).} \tag{5.4}$$

This boundary condition fixes the concentration distribution and slip velocity. In the following section, we consider how these values relate to motion in the original geometry.

Reciprocal Theorem Because the solute distribution at zero Péclet number is harmonic, it is conformally invariant. The resulting slip velocity over the particle's surface is invariant as well, but the corresponding global flows are not, since their stream functions are not generally harmonic. This implies that the swimming speed, accurate up to

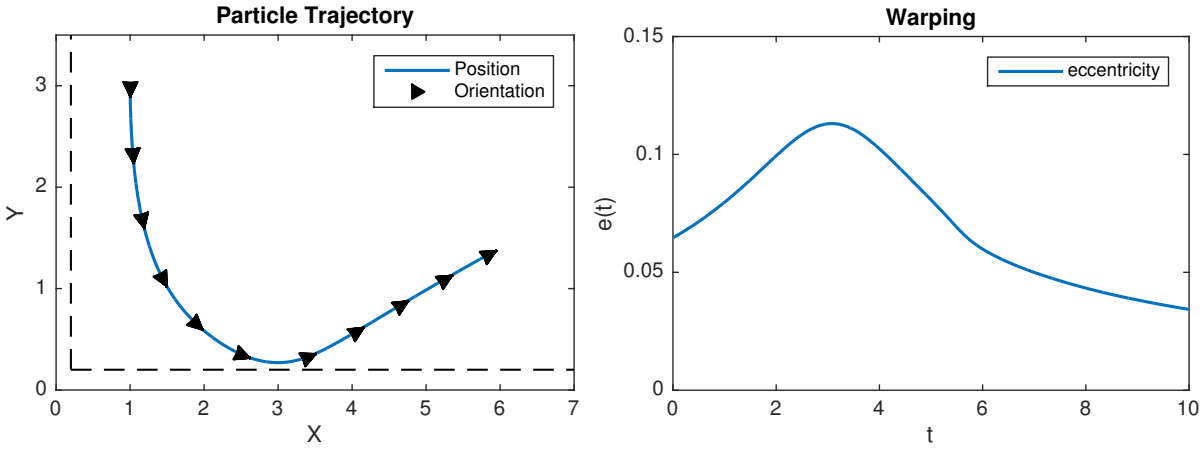

(a) (b)

Figure 13: (a) The numerically simulated trajectory of a two-dimensional Janus particle near a corner. Orientation is marked by arrowheads at $t = 1, 2$, etc. The swimmer re-orients away from confining walls, as has been seen in previous sections. (b) The magnitude of mapping-induced warping is estimated by the eccentricity e. In this case, while the warping is never large, it becomes smaller as the particle leaves the corner.

the effects of warping, must be obtained by applying the reciprocal theorem to the slip velocity and appropriate dragging problem within the original geometry. In general, the dragging problem in bounded two-dimensional geometries is not easily solved.

For simplicity, I choose to approximate this process by employing Crowdy's solution within the half-plane, effectively applying the reciprocal theorem in the new geometry as though the global flows were invariant. While the results are therefore not rigorous, the invariance of the slip velocity suggests they could be qualitatively correct, providing insight into the particle dynamics of the original geometry. The procedure is as follows.

Procedure Given a particle in some geometry, I map the entire region to the upper half plane and compute the effective values Y_{eff}, s_{eff}, θ_{eff}, χ_{eff}, and a_{eff} defined above. By substituting these into Crowdy's equations of motion (4.69), I calculate the velocity and rotation rate of the particle within the half plane. After propagating the mapped particle one time step forward, I relate the new position and orientatioin to the original geometry by applying the inverse mapping and calculating the positions of the centroid, z_α and z_β. Repeating this process for many time steps yields a trajectory. Below, I apply this procedure to a particle in a corner and a semi-infinite channel.

Corner The first extension of Crowdy's solution I attempt is the particle near a corner consisting of walls on the positive x and y axes. The first quadrant is mapped to the upper half plane by the function $f(z) = z^2$. Using this mapping with the above procedure, I have simulated the motion of a particle with $s = 0.2$, $a = -1$, and $\chi = \pi$, initially at the position $(X, Y) = (1, 3)$ and orientation $\phi = -\pi/2$. The resulting trajectory is presented in Fig. 13. As in the half plane case, the particle rotates away from confining walls; broadly, it is likely that Janus swimmers near corners re-orient away from their confinement. The warping is never large and falls off with distance from the origin.

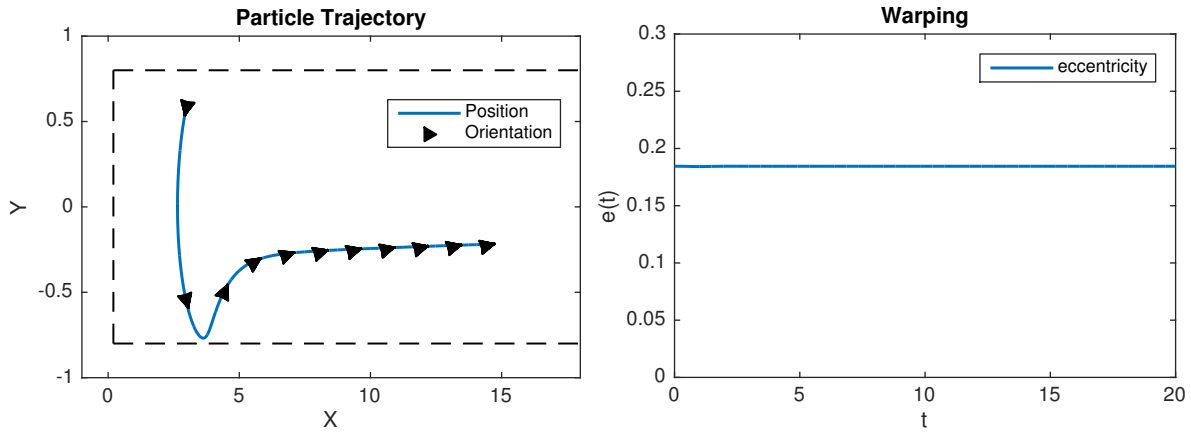

(a) (b)

Figure 14: (a) The numerically simulated trajectory of a two-dimensional Janus particle in a semi-infinite channel. Orientation is marked by arrowheads at $t = 2, 4$, etc. A build-up of solute on the particle's left side appears to continuously orient the swimmer down the channel. (b) The magnitude of mapping-induced warping is estimated by the eccentricity e. In this case, the warping is effectively constant, even far from the origin.

Semi-Infinite Channel The second extension is a particle within a semi-infinite channel, with walls on $y = \pm 1$ and $x = 0$. In this case, the function

$$f(z) = \cosh\left(\frac{\pi(z+i)}{2}\right) \tag{5.5}$$

maps the channel to the upper half plane. Using this mapping, I have simulated the motion of a particle with $s = 0.2$, $a = -1$, and $\chi = \pi$, initially at the position $(X, Y) = (3, 0.6)$ and orientation $\phi = -4\pi/5$. The resulting trajectory is shown in Fig. 14. As before, the particle is rotated away from walls. It appears that a build-up of solute on the particle's left works to orient the swimmer down the channel. Rather than sinusoidally swimming about the channel midplane, the particle asymptotically approaches $y = 0$ as x increases. The small warping from the mapping is effectively constant.

6 Conclusions and Future Work

Conclusions Janus particles with positive mobility show more complex behavior near walls than their negative-mobility counterparts, which always make contact in finite time. The conclusions below describe the dynamics of the former.

Confinement Avoidance The leading-order effect on a Janus particle near a wall is a normally-directed repulsion which scales with the source part of the swimmer's surface activity. In contrast, the unbounded swimming speed and subdominant confinement effects scale with the dipole portion of the activity. This suggests particle behavior can be tuned by altering the relative strength of the source and dipole activity coefficients. Note that the two parameters are not independent if one of the swimmer faces is inert, as in the analysis of Ibrahim and Liverpool [13].

In most situations, hydrodynamic reactions induce a rotation away from wall. The strength of this effect increases sharply as the particle approaches, causing the swimmer

to rapidly re-orient towards open fluid. Frequently, collisions are avoided by this process. If the particle faces are equal sizes, the direction of rotation is the same for all positions and orientations. More generally, if the face with higher surface activity is much larger than the other, some orientations cause a rotation towards the wall.

For equal cap sizes, the combined repulsion and rotation leads swimmers to generally avoid confining walls. This suggests particles in bounded environments are likely to congregate in central, open areas, as seen in the semi-infinite channel shown in Fig. 14. If this effect holds when multiple swimmers are present, the resulting induced proximity could cause enhanced or accelerated inter-particle dynamics, such as the formation of multi-particle structures through clumping [9].

Wall Capture This essay found no stable steady states for particles of equal cap size. As explained above, the work of Crowdy [10] shows that some orientations of swimmers with unequal cap sizes cause rotation towards the wall. This implies the existence of situations in which there is no rotation at all, providing indirect evidence for the sliding state observed by Uspal et al. [4]. Janus particles with unequal cap sizes may be susceptible to capture by confining walls, where the swimmer translates steadily along the boundary. This may be desired; consider a particle which must take the left path at a fork in a channel. Capture by the left channel wall will yield the correct behavior.

It is likely that particles could be designed with similar specific purposes in mind. Imagine, for instance, that a Janus swimmer is desired to be captured and translate at a certain height above a boundary, perhaps releasing medication at the optimal distance from a capillary wall. The relative sizes of the particle faces could be carefully chosen to yield a specific orientation at the selected height with no induced rotation. The source strength of the particle's activity distribution could be similarly calibrated to exactly offset any resultant motion towards the wall. This process would yield a particle which behaves exactly as intended.

Future Work

Thermal Noise Throughout the essay, there is no mention of thermal noise, which continuously works to randomly re-orient swimming particles. The degree to which the equations of motion derived by Ibrahim and Liverpool (3.37) and Crowdy (4.69) are robust against this process should be investigated. Of particular interest is the length of time a particle is expected to remain in the sliding state observed by Uspal et al. [4].

Surface Chemistry While the fixed-flux boundary condition used in this analysis is convenient, more accurate descriptions of the particle surface chemistry would yield more realistic swimmer behavior. The surface activity A likely depends on the concentration of at least one fuel source c_{fuel}. An accurate treatment would consider the global fuel distribution, and the effects of confinement on its diffusion would likely have a large impact on the resulting particle behavior.

Near Wall Behavior While the two-dimensional particle near a wall was solved exactly in Crowdy's analysis [10], Ibrahim and Liverpool [13] employed an approximation in the three-dimensional case which broke down as the particle approached the wall. The particle trajectories explored in Fig. 6, for instance, feature turning points at positions

where errors can reach the order of 20% or higher. A lubrication-style analysis, where derivatives are scaled as in the "inner region" portion of §2.3, could reveal more accurate behavior when the particle is near the wall.

Unequal Caps in Three Dimensions Ibrahim and Liverpool [13] limited their analysis to Janus particles of equal cap size and constant mobility, as this configuration is well approximated by a linear activity function. This approach could be expanded to more general cap sizes by computing the Legendre coefficients of the corresponding activity distributions A and considering higher-order terms of the resulting solute concentration and bulk flow. As an example, the first three coefficients for the distribution

$$A(\theta) = \begin{cases} A^+, & 0 < \theta < \theta_0, \\ A^-, & \theta_0 < \theta < \pi, \end{cases} \tag{6.1}$$

are given by the following relations

$$\begin{aligned} A_0 &= \frac{1}{2}\left[A^+ + A^- + \left(A^- - A^+\right)\cos\theta_0\right], \\ A_1 &= \frac{3}{4}\left(A^+ - A^-\right)\sin^2\theta_0, \\ A_2 &= \frac{5}{4}\left(A^+ - A^-\right)\cos\theta_0\sin^2\theta_0, \end{aligned} \tag{6.2}$$

which recover the correct values for $\theta_0 = \pi/2$. Note that A_2 changes sign depending on the value of θ_0, suggesting it could be responsible for more complex behavior than that observed for A_0 and A_1 at $\theta_0 = \pi/2$. In particular, this analysis could explicitly reveal the existence of the sliding state observed by Uspal et al. [4].

References

[1] Taylor, G., 1951, November. Analysis of the swimming of microscopic organisms. In *Proceedings of the Royal Society of London A: Mathematical, Physical and Engineering Sciences* (Vol. 209, No. 1099, pp. 447-461). The Royal Society.

[2] Purcell, E.M., 1977. Life at low Reynolds number. *Am. J. Phys, 45*(1), pp.3-11.

[3] Popescu, M.N., Dietrich, S. and Oshanin, G., 2009. Confinement effects on diffusiophoretic self-propellers. *The Journal of chemical physics, 130*(19), p.194702.

[4] Uspal, W.E., Popescu, M.N., Dietrich, S. and Tasinkevych, M., 2015. Self-propulsion of a catalytically active particle near a planar wall: from reflection to sliding and hovering. *Soft matter, 11*(3), pp.434-438.

[5] Michelin, S. and Lauga, E., 2015. Autophoretic locomotion from geometric asymmetry. *The European Physical Journal E, 38*(2), pp.1-16.

[6] Golestanian, R., Liverpool, T.B. and Ajdari, A., 2007. Designing phoretic micro-and nano-swimmers. *New Journal of Physics, 9*(5), p.126.

[7] Anderson, J.L., 1989. Colloid transport by interfacial forces. *Annual review of fluid mechanics, 21*(1), pp.61-99.

[8] Walther, A. and Müller, A.H., 2008. Janus particles. *Soft Matter, 4*(4), pp.663-668.

[9] Sciortino, F., Giacometti, A. and Pastore, G., 2010. A numerical study of one-patch colloidal particles: from square-well to Janus. *Physical Chemistry Chemical Physics, 12*(38), pp.11869-11877.

[10] Crowdy, D.G., 2013. Wall effects on self-diffusiophoretic Janus particles: a theoretical study. *Journal of Fluid Mechanics, 735*, pp.473-498.

[11] Ghosh, P.K., Misko, V.R., Marchesoni, F. and Nori, F., 2013. Self-propelled Janus particles in a ratchet: Numerical simulations. *Physical review letters, 110*(26), p.268301.

[12] Ao, X., Ghosh, P.K., Li, Y., Schmid, G., Hnggi, P. and Marchesoni, F., 2015. Diffusion of chiral Janus particles in a sinusoidal channel. *EPL (Europhysics Letters), 109*(1), p.10003.

[13] Ibrahim, Y. and Liverpool, T.B., 2015. The dynamics of a self-phoretic Janus swimmer near a wall. *EPL (Europhysics Letters), 111*(4), p.48008.

[14] Stone, H.A. and Samuel, A.D., 1996. Propulsion of microorganisms by surface distortions. *Physical review letters, 77*(19), p.4102.

[15] Squires, T.M. and Bazant, M.Z., 2006. Breaking symmetries in induced-charge electro-osmosis and electrophoresis. *Journal of Fluid Mechanics, 560*, pp.65-101.

[16] Blake, J.R. and Chwang, A.T., 1974. Fundamental singularities of viscous flow. *Journal of Engineering Mathematics, 8*(1), pp.23-29.

[17] Crowdy, D., 2011. Treadmilling swimmers near a no-slip wall at low Reynolds number. *International Journal of Non-Linear Mechanics, 46*(4), pp.577-585.

[18] Crowdy, D., 2008. The Schwarz problem in multiply connected domains and the Schottky-Klein prime function. *Complex Variables and Elliptic Equations, 53*(3), pp.221-236.